De novo formation and maintenance of mammalian peroxisomes in the absence of PEX16

Yuichi Yagita[1,§], Yuichi Abe[2], and Yukio Fujiki[1,3,4,*]

[1]Division of Organelle Homeostasis, Medical Institute of Bioregulation, Kyushu University, 3-1-1 Maidashi, Fukuoka 812-8582, Japan;
[2]Faculty of Arts and Science, Kyushu University, 744 Motooka Nishi-ku, Fukuoka 819-0395, Japan;
[3]Institute of Rheological Functions of Food-Kyushu University Collaboration Program, Kyushu University, Fukuoka 812-8582, Japan;
[4]Graduate School of Science, University of Hyogo, Hyogo 678-1297, Japan

*Corresponding author, Tel.: +81-92-642-4232; fax: +81-92-642-4233
E-mail address: yfujiki@kyudai.jp (Y. Fujiki)
[§]Y. Yagita's present address is MRC Laboratory of Molecular Biology, Francis Crick Avenue, Cambridge CB2 0QH, UK.

Key words
Peroxisome, Peroxisomal membrane biogenesis, PEX16

Summary statement
In contrast to *PEX16*-deficient fibroblasts from Zellweger syndrome patients, PEX16-knockout HeLa, HEK293, and CHO-K1 cell lines established using the CRISPR/Cas9 system can partially maintain peroxisomes.

Abstract
Mammalian PEX16 has been considered essential for generating and maintaining peroxisomal membranes. This view is based primarily on the finding that fibroblasts from several *PEX16*-deficient patients are devoid of peroxisomal structures, but can form peroxisomes upon expression of PEX16. However, unlike these patient-derived cells, *pex16* mutants in other model organisms contain partially functional peroxisomes. Here, we report that PEX16-KO cells derived from three mammalian cultured cell lines are comprised of cells containing a fewer number of enlarged peroxisomes and cells lacking peroxisomes. We also suggest that PEX16 accelerates the process by which peroxisome-less cells form peroxisomal membranes and subsequently establish mature peroxisomes,

independently on its ability to mediate peroxisomal targeting of PEX3. Nevertheless, PEX16 is not absolutely required for this process. Moreover, a well-known patient-derived PEX16 mutant inhibits the *de novo* formation of peroxisomal membranes. Our findings suggest that although PEX16 is undoubtedly important for optimal peroxisomal membrane biogenesis, mammalian cells may be able to form peroxisomes *de novo* and maintain the organelles without the aid of PEX16.

Abbreviations used in this paper: CHO, Chinese hamster ovary; DKO, double-KO; PBD, peroxisome biogenesis disorder; PMP, peroxisomal membrane protein; PTS1, peroxisomal targeting signal 1; ZS, Zellweger syndrome.

Introduction

Peroxisomes are single membrane-enclosed organelles that fulfill a diverse range of metabolic functions, including fatty acid oxidation and ether lipid synthesis (Wanders and Waterham, 2006). These versatile organelles depend on a set of peroxins encoded by the *PEX* genes for their biogenesis. Mutations in the *PEX* genes impair peroxisome assembly, leading to the defects in peroxisomal metabolic pathways, which in humans cause peroxisome biogenesis disorders (PBDs) (Wanders, 2014).

Fibroblasts derived from the vast majority of PBD patients contain aberrant peroxisomes that have an array of peroxisomal membrane proteins (PMPs), but not matrix proteins. By contrast, fibroblasts from a rare subset of PBD patients are devoid of any detectable peroxisomal membranes, and these patients are associated with mutations in the *PEX3*, *PEX16*, or *PEX19* genes (Fujiki et al., 2014; Waterham et al., 2016). Likewise, *PEX3*- or *PEX19*-deficient mammalian cells obtained by means of mutagenesis or targeted KO have been reported to lack peroxisomal membranes (Kinoshita et al., 1998; Matsuzono et al., 1999; Ghaedi et al., 2000; Schrul and Kopito, 2016; Jean Beltran et al., 2018; Tanaka et al., 2019). Notably, these peroxisome-less cells can form peroxisomes *de novo* upon introduction of the respective wild-type genes (Agrawal and Subramani, 2016; Farré et al., 2019). Previous studies on mammalian PEX3, PEX16, and PEX19 have established their roles in the biogenesis of PMPs (Fang et al., 2004; Jones et al., 2004; Kim et al., 2006; Matsuzaki and Fujiki, 2008; Yagita et al., 2013; Hua et al., 2015; Liu et al., 2016). Thus, the impaired PMP biogenesis seems to ultimately result in the loss of peroxisomal membranes.

It has long been considered that PEX3 and PEX19 are highly conserved across eukaryotes, while PEX16 is not. Indeed, despite its initial identification in the yeast *Yarrowia lipolytica* (Eitzen et al., 1997), the *PEX16* gene is absent in most yeast species (Schlüter et al., 2006; Smith and Aitchison, 2013). Moreover, unlike mammalian PEX16, *Y. lipolytica* Pex16 has been suggested to function in peroxisome division (Eitzen et al., 1997; Guo et al., 2003; Guo et al., 2007). However, a more recent

study reported that *Komagataella phaffii* (formerly called *Pichia pastoris*) Pex36 and *Saccharomyces cerevisiae* Pex34 are functionally homologous to PEX16 (Farré et al., 2017). Intriguingly, the growth defect phenotype of *K. phaffii pex36*Δ cells can be rescued partially by overexpressing human PEX16, *Y. lipolytica* Pex16, or *S. cerevisiae* Pex34; while *K. phaffii* Pex36 is capable of inducing *de novo* peroxisome formation in *PEX16*-defective human fibroblasts (Farré et al., 2017). Thus, PEX16 orthologues might be more conserved than previously thought and share some functional similarity.

Nevertheless, dysfunction of PEX16 orthologues does not necessarily lead to complete loss of peroxisomes. In fungi, *Y. lipolytica pex16*Δ, *Penicillium chrysogenum pex16*Δ, and *K. phaffii pex36*Δ cells can still assemble import-competent peroxisomes (Eitzen et al., 1997; Farré et al., 2017) (Opaliński et al., 2012). Similarly, *Drosophila melanogaster pex16* mutants are able to maintain partially functional peroxisomes (Nakayama et al., 2011). Furthermore, *Arabidopsis thaliana pex16* mutants with negligible levels of PEX16 protein harbor a fewer number of enlarged peroxisomes (Burkhart et al., 2019). Eventually, the complete loss of peroxisomes due to PEX16 deficiency is evident only in the fibroblasts from a few PBD patients (Honsho et al., 1998; Shimozawa et al., 2002; Shaheen et al., 2011).

To address this issue, we reevaluated the consequences of PEX16 disruption in mammalian cells by generating and analyzing PEX16-KO clonal cells derived from three widely used cultured cell lines. We suggest that PEX16 is unequivocally pivotal for optimal peroxisome biogenesis, but is not a prerequisite for assembling peroxisomes *de novo* or maintaining them. Our observations are rather consistent with the previous studies on non-mammalian model organisms, challenge the current view that mammalian PEX16 is absolutely essential for peroxisomal membrane biogenesis, and might open new avenues for future studies on the mechanisms underlying *de novo* formation and maintenance of peroxisomes.

Results

PEX16-KO HeLa cells can partially maintain import-competent peroxisomes

To reexamine the biogenesis of peroxisomes in *PEX16*-defective human cells, we generated PEX16-KO HeLa cells via the CRISPR/Cas9 system. HeLa cells were used, since PEX3 or PEX19 KO in HeLa cells results in loss of peroxisomal membranes (Schrul and Kopito, 2016; Baldwin et al., 2021; unpublished data; see also later sections). By targeting exon 1, we established multiple PEX16-KO clonal HeLa cell lines, from which four representative clones were used in this study (Fig. S1A). Immunoblot analysis using total cell lysates and membrane fractions prepared from these PEX16-KO clones showed no detectable PEX16 protein (Fig. 1A). These PEX16-KO cell lines were then immunostained for PMP70 (also known as ABCD3) and catalase, markers for the peroxisomal membrane and matrix proteins, respectively. Strikingly, all the cell lines were heterogeneous in terms

of peroxisome biogenesis; a subpopulation of cells showed PMP70- and catalase-containing peroxisomes, whereas the rest of cells lacked PMP70-positive structures with catalase being localized diffusively in the cytosol (Fig. 1B). The proportions of cells harboring peroxisomes varied between the clones (Fig. 1C). Intriguingly, the heterogeneous biogenesis of peroxisome was still observed in subclones established from two PEX16-KO cell lines (Fig. 1D; Fig. S1B), implying that the complete loss of peroxisomes may occur stochastically. In addition, peroxisomes in PEX16-KO cells were larger in size and fewer in number than those in wild-type cells (Fig. 1B, insets; Fig. 1E), suggesting impaired peroxisome biogenesis even in these peroxisome-positive cells. We also performed quantitative RT-PCR and demonstrated that the steady-state *PEX16* mRNA expression was decreased by ~40–90% in PEX16-KO clones (Fig. S1C), implying that the mutations trigger nonsense-mediated mRNA decay. Apparently, although the level of *PEX16* mRNA expression differs among clones, this difference did not explain the difference in the proportion of peroxisome-positive cells.

PEX16-KO HEK293 and CHO-K1 cells exhibit heterogeneous peroxisome biogenesis

To validate the peroxisomal phenotypes observed in PEX16-KO HeLa cells, we generated additional KO cells using the human embryonic kidney cell line HEK293 and the Chinese hamster ovary (CHO)-derived cell line CHO-K1, both of which have been widely used in cell biology. For KO in HEK293 cells, we used two gRNAs that were the same as those used for the KO in HeLa cells and three additional gRNAs that were designed to target exon 4, and analyzed one representative clone for each gRNA (Fig. S2A). PEX16 protein was not detectable in the five PEX16-KO clonal HEK293 cell lines (Fig. S2B). Decrease in the steady-state *PEX16* mRNA level was also observed in these KO clones, with clones ex1-g1-14 and ex1-g2-6, which were generated by disrupting exon 1, showing a prominent decrease (Fig. S2C). Importantly, all the PEX16-KO HEK293 clones were comprised of cells with peroxisomes and cells lacking peroxisomes (Fig. 2A,B), and peroxisomes found in the KO cells were fewer in number and larger in size (Fig. 2C).

Similar peroxisomal phenotypes were observed in two Pex16-KO CHO-K1 clonal cell lines generated using independent gRNAs targeting exon 4 (Fig. 3; Fig. S3). Unfortunately, due to difficulty in detecting endogenous Pex16 protein in CHO-K1 cells by immunoblotting, we were unable to present evidence for lack of Pex16 protein expression in these CHO-K1-derived cell lines. For clone ex4-g1-6, we failed to determine the mutation(s); nevertheless, the result of quantitative RT-PCR analysis suggests that this clone is likely to have a large deletion around exon 4 (Fig. S3), which encodes a putative transmembrane domain that was shown to be required for peroxisomal localization and function of PEX16 (Honsho et al., 2002). Apparently, this clone exhibited rather more severe phenotypes than the other CHO-K1-derived clone ex4-g2-21. For instance, peroxisomes in ex4-g2-21 were positive for both catalase and a subset of peroxisomal matrix proteins harboring peroxisomal targeting signal 1 (PTS1), while those in ex4-g1-6 cells were positive for the latter

proteins, but barely for catalase (Fig. 3A,B). Thus, it is unlikely that clone ex4-g1-6 expresses a functional Pex16 protein.

Reintroduction of the PEX16 gene rescues the peroxisomal phenotypes in PEX16-KO cell lines

To exclude the possibility that the aberrant peroxisome biogenesis in PEX16-KO cells was due to off-target effects, we sought to perform rescue experiments by expressing wild-type PEX16. During the course of this study, we realized that PEX16 overexpression in wild-type HeLa cells often induced complete loss of peroxisomes or resulted in cells with fewer and often larger peroxisomes, irrespective of whether PEX16 was epitope-tagged or not (Fig. S4). The disruption of peroxisome biogenesis induced by PEX16 overexpression was also observed in HEK293 and CHO-K1, although it was not as severe as in HeLa cells. Consistently, a similar observation was recently reported in HeLa, HEK293T, and U2OS cells stably overexpressing PEX16 (Baldwin et al., 2021). We therefore optimized DNA transfection conditions such that exogenous PEX16 expression had little impact on peroxisome morphology in wild-type cells (Fig. S4). As a result, HA-PEX16 expressed in wild-type as well as in PEX16-KO HeLa cells was barely visible by immunofluorescence microscopy; the detectable HA-PEX16 signals colocalized almost exclusively with PMP70 (Fig. 4A; Fig. S5A). Importantly, this low-level expression of HA-PEX16 rescued the aberrant peroxisome morphology in PEX16-KO HeLa clone ex1-g1-3, which was evident even in cells where the HA-PEX16 levels were under detectable (Fig. 4A; Fig. S5A). A similar observation was made in the other PEX16-KO HeLa clones upon HA-PEX16 expression (Fig. S5B,C). To further support this observation, we quantified the number and size of peroxisomes in PEX16-KO cells after expression of PEX16. For this, we employed a viral 2A sequence-based bicistronic vector encoding HA-PEX16 and mCherry fused with nuclear localization signals (mCherryNLS), facilitating the identification of transfectants. Indeed, the quantification confirmed that the low-level expression of PEX16 rescued the aberration in peroxisome morphology in PEX16-KO HeLa, HEK293, and CHO-K1 clones, as assessed by immunostaining for PMP70 (Fig. 4B–D; Fig. S5B–D). Next, we asked if the transient expression of PEX16 can increase the proportion of cells with peroxisomes in PEX16-KO cells. To this end, we used PEX16-KO HeLa ex1-g1-20 subclones 3 and 6, which showed a lower number of cells with peroxisomes. At 4 days after transfection, we analyzed the cells for the presence of peroxisomes and demonstrated a significant increase in the proportion of peroxisome-positive cells (Fig. 4F). Thus, it is most likely that the impaired peroxisome biogenesis in PEX16-KO cells was accounted for by the PEX16 deficiency.

Taken together, these observations suggest that although the CRISPR/Cas9-mediated KO of PEX16 in HeLa, HEK293, and CHO-K1 cells has a significant impact on peroxisome biogenesis, these mammalian cultured cells can manage to maintain import-competent peroxisomes in the absence of PEX16.

PEX3 localizes to peroxisomes in PEX16-KO HeLa cells but with reduced efficiency

Mammalian PEX16 has been suggested to function in the biogenesis of PEX3 (Kim et al., 2006; Matsuzaki and Fujiki, 2008; Hua et al., 2015). Given the essential role of PEX3 in the import of most PMPs (Fang et al., 2004; Matsuzono and Fujiki, 2006; Yagita et al., 2013; Liu et al., 2016), the presence of peroxisomes in PEX16-KO mammalian cultured cells implied that PEX3 would localize to peroxisomes without the aid of PEX16. Indeed, endogenous PEX3 was localized to peroxisomes in PEX16-KO cells with catalase-positive peroxisomes (Fig. 5A). It should be noted that PEX3 was not visible in PEX16-KO cells lacking catalase-positive puncta (Fig. 5A); whether the lack of detectable PEX3 in these cells is a cause or effect of the complete loss of peroxisomal membranes is to be determined.

We also assessed the peroxisomal targeting of nascent PEX3 in PEX16-KO HeLa cells by transiently expressing PEX3-HA. The result revealed that PEX3-HA was colocalized with PMP70 (Fig. 5B). However, almost all transfected cells also displayed an mislocalization of PEX3-HA to cytoplasmic compartments, potentially to the ER and/or mitochondria. Our transfection conditions were optimized to express PEX3-HA at a relatively low level, and under the same transfection conditions, PEX3-HA was almost exclusively localized to peroxisomes in wild-type HeLa cells, with <1% cells showing mislocalization of PEX3-HA to mitochondria (data not shown). Furthermore, as described in the following section, a similar partial cytoplasmic mislocalization was also observed for PEX3 that was stably expressed in the PEX16-KO background (Fig. 6F). Thus, the observed mislocalization of PEX3-HA in PEX16-KO HeLa cells seemed not to be a simple artifact caused by overexpression. In addition to this mislocalization, we also noticed that at least in some cells, not all peroxisomes efficiently incorporated PEX3 (Fig. 5B, middle panels). Collectively, these observations suggest that PEX3 can localize to peroxisomes with a lower efficiency in the absence of PEX16.

PEX16 is not essential for but facilitates de novo peroxisome formation

Since mammalian PEX16 is thought to be indispensable for *de novo* peroxisome formation (Kim et al., 2006; Sugiura et al., 2017; Farré et al., 2019), we next set out to investigate whether the *de novo* peroxisome assembly observed upon complementation of peroxisome-less cells requires PEX16. To this end, we disrupted the *PEX3* and *PEX19* individually in PEX16-KO clone ex1-g1-3 cells (Fig. S6A). The resulting double KO (DKO) cell lines, PEX16/PEX3-DKO and PEX16/PEX19-DKO, respectively, were confirmed to lack peroxisomal membranes by immunostaining for PMP70 (Fig. S6B). Using these cell lines, we then performed genetic complementation assays and asked whether peroxisomes arise.

PEX16/PEX3-DKO cells were transfected with *HA-PEX16*, *PEX3*, or both together. At 48 h post-transfection (Fig. S6C), *PEX3*-transfected cells showed a very few PMP70-positive puncta that were negative for catalase, whereas transfectants with *PEX3* and *HA-PEX16* exhibited more PMP70-positive puncta that occasionally coincided with catalase. Remarkably, at 64 h post-transfection (Fig.

6A,B), *PEX3*-tranefected cells displayed several PMP70-containing structures that were either positive or still negative for catalase, while cells transfected with both *PEX3* and *HA-PEX16* established numerous import-competent peroxisomes. On the other hand, the transfection of *HA-PEX16* alone failed to generate any peroxisomal structures (Fig. 6A; Fig. S6C). Similar observations were made using PEX16/PEX19-DKO cells upon expression of FLAG-PEX19 (Fig. 6C,D), except that the progression of the PEX19-induced peroxisome formation appeared to be slower than that of the PEX3-induced one in PEX16/PEX3-DKO cells; at 64 h post-transfection, the transfection of *FLAG-PEX19* resulted in formation of one to several PMP70-positive, but catalase-negative, structures (Fig. 6C). The physiological significance of and reason for this difference remains unclear. Given that PEX3-containing pre-peroxisomal structures are thought to be fundamental to the formation of mature peroxisomes (Agrawal and Subramani, 2016; Farré et al., 2019), one possible explanation could be that PEX3 overexpression generated many PEX3-positive structures that later imported other PMPs and matrix proteins, leading to the apparently faster progression.

To further confirm that import-competent peroxisomes can arise *de novo* in the PEX16-KO background, especially in PEX16/PEX19-DKO cells, we generated PEX16/PEX19-DKO cells stably expressing HA-PEX19 using puromycin as a selection marker. The established cell line, termed 16/19-DKO$^{\text{HA-PEX19}}$, was a bulk population of puromycin-resistant cells, and therefore not all cells expressed HA-PEX19. Importantly, a subpopulation of the HA-PEX19-expressing cells contained catalase-positive peroxisomes (Fig. 6E), providing further evidence for the PEX16-independent *de novo* assembly of peroxisomes. The presence of peroxisomes was likewise evident in a subpopulation of the PEX16/PEX3-DKO cells stably expressing PEX3-mEGFP (Fig. 6E). In this cell line, termed 16/3-DKO$^{\text{PEX3-mEGFP}}$, a portion of PEX3-mEGFP showed a cytoplasmic, non-peroxisomal localization (Fig. 6F), further implying the importance of PEX16 for the PEX3 biogenesis. Collectively, our findings suggest that PEX16 is not essential for *de novo* peroxisome biogenesis involving the initial formation of pre-peroxisomal membranes, but is nevertheless likely to enable peroxisome-less cells to efficiently generate hundreds of peroxisomes upon genetic complementation.

C-terminal part of PEX16 is important for its ability to accelerate de novo peroxisome biogenesis

To gain insight into how PEX16 accelerates the process by which numerous peroxisomes are established in cells lacking pre-existing peroxisomes (Fig. 6), we focused on two well-characterized PEX16 mutants: PEX16ΔN69 and PEX16R176X (Fig. 7A). PEX16ΔN69 lacks the N-terminal 69 aa residues (Honsho et al., 2002). PEX16R176X (or p.Arg176Ter) was identified in a patient with Zellweger syndrome (ZS) (Honsho et al., 1998; South and Gould, 1999), the most severe form of PBD. Notably, the fibroblast cell line established from this patient (known as GM06231) lacks peroxisomal membranes and has been commonly used in this research field. Our earlier study showed that both PEX16ΔN69 and PEX16R176X can localize to peroxisomes, but cannot restore peroxisome

assembly in GM06231 cells (Honsho et al., 2002). In addition, our later *in vitro* study suggested that PEX16ΔN69 is unable to mediate peroxisomal targeting of PEX3 (Matsuzaki and Fujiki, 2008). Although not determined experimentally, PEX16R176X is supposed to be defective in mediating the PEX3 targeting, since a mutant lacking the C-terminal 21 aa residues is devoid of this activity (Matsuzaki and Fujiki, 2008).

We examined whether these two mutants can accelerate the peroxisome assembly in PEX16/PEX19-DKO HeLa cells. Surprisingly, PEX16ΔN69 retained the ability to facilitate the PEX19-induced formation of peroxisomes (Fig. 7B–D). Quantification analysis suggested that PEX16ΔN69 facilitated the PEX19-induced *de novo* peroxisome formation as efficiently as wild-type PEX16 did, although the formation of mature peroxisomes tended to be less efficient in *PEX16ΔN69*-transfected cells than in *PEX16*-transfected cells (Fig. 7E). Furthermore, we also demonstrated that PEX16ΔN69 can rescue the aberrant peroxisomal morphology in PEX16-KO HeLa cells (Fig. S6D,E). These results imply that PEX16 exerts an as yet unknown function when peroxisome-less cells establish numerous peroxisomes upon complementation. By contrast, PEX16R176X failed to accelerate the PEX19-induced de novo formation of peroxisomes. PEX16R176X rather appeared to inhibit the generation of PMP70-contatining structures (Fig. 7B, rightmost panel). To confirm this, we performed a similar experiment in PEX16/PEX3-DKO HeLa cells, which can form more peroxisomes upon expression of PEX3 alone than PEX16/PEX19-DKO can upon expression of PEX19 alone (Fig. 6). The results indicated that PEX16R176X significantly decreased the number of cells that formed PMP70-positive structures (Fig. 7F–H), supporting the notion that PEX16R176X can abrogate *de novo* peroxisome biogenesis. Although the underlying mechanism remains to be addressed, this finding seems to be consistent with our previous result that PEX16R176X overexpression in CHO-K1 cells affected peroxisome biogenesis (Honsho et al., 2002), paradoxically suggests the involvement of PEX16 in the formation of peroxisomal membranes, and might provide clues to why a few of the reported *PEX16*-deficient fibroblasts are devoid of peroxisomes. Altogether, our results argue that the C-terminal part of PEX16 plays a previously unknown and yet important role in the biogenesis of peroxisomes.

Discussion

The present study has suggested that PEX16 is unambiguously important for peroxisome biogenesis in HeLa, HEK293, and CHO-K1, but also suggested that these mammalian cultured cells manage to form and maintain peroxisomes in the absence of PEX16. Thus, our findings appear to challenge the long-standing view that mammalian PEX16 is an absolute requirement for *de novo* peroxisome formation (Kim and Mullen, 2013). Nonetheless, our observations are in good agreement with reports on the PEX16 orthologue mutants in other model systems (Burkhart et al., 2019) (Eitzen et al., 1997;

Nakayama et al., 2011; Opaliński et al., 2012; Farré et al., 2017). Moreover, the presence of import-competent peroxisomes in our PEX16-KO cells might explain why our extensive genetic screening of peroxisome-deficient CHO cell mutants has not isolated any mutants defective in the *Pex16* gene (Fujiki et al., 2020).

Previous studies reported that fibroblasts from *PEX16*-deficient ZS patients are devoid of peroxisomes (Honsho et al., 1998; Shimozawa et al., 2002; Shaheen et al., 2011). On the other hand, the PEX16-KO clonal cell lines established in the present study were a mixture of cells with import-competent peroxisomes and cells without peroxisomal membranes (Figs. 1–3; Figs. S1–S3). As our knowledge on the function of PEX16 and more broadly on peroxisome biogenesis is limited, it is difficult to reconcile the difference between these observations. Given the apparently mild phenotypes of our PEX16-KO cells, one might speculate that these KO cells would still express partially functional PEX16 protein. However, similar peroxisomal phenotypes were confirmed in multiple KO clones generated from three different cell lines, two human and one Chinese hamster cell lines, using multiple gRNAs targeting exon 1 or exon 4. Furthermore, immunoblot analysis using the antibody against the C-terminal ~90 residues of human PEX16 showed no detectable full-length or truncated PEX16 protein at least in the human cell-derived PEX16-KO clones (Fig. 1A and Fig. S2B), and nonsense-mediate mRNA decay was evident in many of the PEX16-KO clones, especially in the clones generated by disrupting exon 1 (Figs. S1–S3). Thus, it seems unlikely that our PEX16-KO cells have a hypomorphic allele. Nevertheless, we cannot completely exclude the possibility that these PEX16-KO clones express a truncated PEX16 protein at an undetectable level. In that scenario, however, expression of a truncated PEX16 would not necessarily lead to a milder phenotype and could potentially result in a more severe phenotype than a null phenotype. Importantly, a similar scenario could happen also in the *PEX16*-deficient ZS fibroblasts; the disease-causing mutations in the ZS fibroblasts might contribute to the complete loss of peroxisomes, as implied by an inhibitory effect of PEX16R176X on peroxisome biogenesis (Fig. 7) (Honsho et al., 2002). Of note, the *PEX16*-deficient ZS fibroblasts so far reported were shown to express aberrant *PEX16* mRNAs (Honsho et al., 1998; Shimozawa et al., 2002; Shaheen et al., 2011). Obviously, further research is required to explain the difference between the *PEX16*-deficient ZS fibroblasts and our PEX16-KO cell lines. Given that the phenotypes of our PEX16-KO cells are consistent with the phenotypes of PEX16 orthologue mutants in non-mammalian species, our findings should motivate additional KO studies using other cell lines as well as analysis of knock-in cell lines carrying a disease-causing mutation.

The present study leaves several other questions unanswered. For instance, it is unclear why PEX16-KO cells are heterogeneous in peroxisome biogenesis. Given the aneuploidy and genetic instability in HeLa, HEK293, and CHO-K1 cells (Adey et al., 2013; Landry et al., 2013; Lin et al., 2014; Vishwanathan et al., 2017; Wurm and Wurm, 2017), it might be possible that subpopulations of cells in a given PEX16-KO clonal cell line differentially express proteins involved in any aspect of peroxisome biogenesis; leading to differential peroxisome biogenesis, including *de novo* formation

and degradation. Intriguingly, a similar heterogeneity was recently reported in *Vdac2*-deficient mouse embryonic fibroblasts (Hosoi et al., 2017) as well as VPS13D-KO HeLa cells (Baldwin et al., 2021), indicating that this type of phenotype is not restricted to PEX16 deficiency. Although the underlying mechanisms have yet to be investigated, neither VDAC2 nor VPS13D appears to be involved directly in the biogenesis of PMPs. Therefore, these observations suggest that under some unknown circumstances, cells could lose peroxisomal membranes even when the machinery for PMP biogenesis is functional. Supporting this notion, Baldwin et al. (2021) also reported some PEX5-KO and PEX14-KO HeLa clones with a subpopulation of cells lacking peroxisomal membranes, despite the fact that both PEX5 and PEX14 are known to be dispensable for PMP biogenesis (Fujiki, 2016). Further investigations at the single-cell level would be required to explain the observed heterogeneity in peroxisome biogenesis.

Another issue is why peroxisomes found in PEX16-KO cells are larger in size and lower in number. Given the proposed function of PEX16 in the biogenesis of PMPs (Kim et al., 2006; Matsuzaki and Fujiki, 2008; Hua et al., 2015), this could be an indirect effect of PEX16 deficiency. With respect to this issue, it is of interest to mention that a fewer number of enlarged peroxisomes were also observed in fibroblasts from *PEX16*-deficient non-ZS patients (Ebberink et al., 2010; Kumar et al., 2018; Zaabi et al., 2019) and also that knockdown of PEX16 was most recently suggested to induce autophagic degradation of peroxisomes (Wei et al., 2021). Furthermore, how PEX16 facilitates the process by which peroxisome-less cells generate numerous peroxisomes also awaits further studies. This function is unlikely dependent on its ability to mediate the targeting of PEX3 (Fig. 7). Possible roles may include to accelerate the formation of pre-peroxisomal membranes, to facilitate a post-targeting step of the PEX3 biogenesis, to mediate lipid incorporation, to regulate peroxisome division, etc. Whatever the exact function is, it is not necessarily essential for *de novo* peroxisome assembly. Addressing these questions should help clarify the functions of mammalian PEX16 and lead to a comprehensive understanding of the mechanisms underlying *de novo* formation and maintenance of peroxisomes.

Materials and Methods

Antibodies

Rabbit antibodies to catalase (against rat catalase) (Tsukamoto et al., 1990), PMP70 (against aa 645-659 of rat PMP70) (Tsukamoto et al., 1990; Kinoshita et al., 1998), PTS1 peptide (against aa 652- 661 of rat acyl-CoA-oxidase) (Otera et al., 1998), PEX3 (against aa 356-373 of human PEX3; affinity-purified for immunostaining) (Ghaedi et al., 2000), PEX16 (against aa 244-336 of human PEX16) (Honsho et al., 2002), and PEX19 (against human PEX19) (Liu et al., 2016), and guinea pig antibodies to PEX14 (against aa 241-376 of rat PEX14) (Mukai et al., 2002) and catalase (against human catalase) (Yagita et al., 2017) were as described. Mouse monoclonal antibodies against β-actin

(6D1; MBL), cytochrome P450 reductase (F-10; Santa Cruz Biotechnology), and HA (16B12; Covance) were purchased. HRP-linked donkey anti-rabbit IgG and sheep anti-mouse IgG antibodies (GE Healthcare) were used as secondary antibodies for immunoblotting. The following fluorescent-labeled secondary antibodies were used for immunostaining: Alexa Fluor 488- or Alexa Fluor 568-conjugated goat anti-rabbit IgG antibodies; Alexa Fluor 488- or Alexa Fluor 647-conjugated goat anti-guinea pig IgG antibodies; and Alexa Fluor 488-conjugated goat anti-mouse IgG antibody (Invitrogen).

Plasmids

All plasmids used in the present study were generated using standard PCR-based techniques and verified by DNA sequencing. Plasmids encoding PEX3 (pcDNAZeo/*RnPEX3*) (Ghaedi et al., 2000), PEX3-HA (pcDNAZeo/*PEX3-HA*) (Yamashita et al., 2014), and FLAG-PEX19 (pcDNAZeo/*FLAG-PEX19*) (Yagita et al., 2013) were as described. For the plasmids expressing HA-PEX16 (pcDNAZeo/*HA-PEX16*), HA-PEX16ΔN69 (pcDNAZeo/*HA-PEX16ΔN69*), and HA-PEX16R176X (pcDNAZeo/*HA-PEX16R176*X), the corresponding *PEX16* cDNA fragments were amplified from pCMVSPORT.HsPEX16 (Honsho et al., 1998) and subcloned into a modified pcDNA3.1/Zeo(+) vector (Invitrogen) encoding an N-terminal 2×HA tag (pcDNAZeo/*HA*) (Yagita et al., 2013).

For the plasmid encoding mCherryNLS (pcDNAZeo/*mCherryNLS*), a DNA fragment coding for an artificial 24-mer peptide containing three copies of the SV40 large T antigen NLS (DPKKKRKVDPKKKRKVDPKKKRKV; NLS sequences are underlined) was inserted into pcDNAZeo/*mCherry* (Okumoto et al., 2018), downstream of and in-frame with the *mCherry* gene, using inverse PCR.

For the coexpression of mCherryNLS and HA-PEX16, FLAG-PEX19, or PEX3, we used a modified 2A peptide-based bicistronic expression system involving a tandem P2A-T2A sequence, which was shown to minimize the generation of unseparated fusion proteins resulting from incomplete ribosomal skipping (Liu et al., 2017; Pan et al., 2017). The amino-acid sequence of the P2A-T2A cassette used is as follows: GSGATNFSLLKQAGDVEENPGPGSGEGRGSLLTCGDVEENPGP (P2A and T2A peptides are underlined). First, a DNA fragment containing the *mCherryNLS* sequence followed in-frame by the P2A-T2A cassette was cloned into pcDNA6N/myc-His A vector, a modified pcDNA6/myc-His A vector (Invitrogen) in which the BglII-NotI fragment containing CMV enhancer/promoter and part of the multiple cloning site had been replaced by the corresponding fragment of pcDNA3.1/Zeo(+) vector. The resulting plasmid, termed pcDNA6N/*mCherryNLS-P2A-T2A*, was then used to create the bicistronic expression plasmids pcDNA6N/*mCherryNLS-2A-HA-PEX16*, pcDNA6N/*mCherryNLS-2A-FLAG-PEX19*, and pcDNA6N/*mCherryNLS-2A-PEX3*. The *HA-PEX16*, *FLAG-PEX19*, and *PEX3* sequences in these plasmids were obtained by PCR from pcDNAZeo/*HA-PEX16*, pcDNAZeo/*FLAG-PEX19*, *and* pcDNAZeo/*RnPEX3*.

For the generation of stable cell lines, we cloned a desired coding sequence into pEF-IRESpuro3 vector (Yagita et al., 2017). To obtain pEF-IRESpuro3/*HA-PEX19*, the *HA-PEX19* sequence was amplified from pcDNAZeo/*HA-PEX19* (Matsuzono et al., 2006) and ligated into pEF-IRESpuro3 vector. To construct pEF-IRESpuro3/*PEX3-mEGFP* expressing PEX3 with a C-terminal mEGFP connected via a 15-aa flexible linker, a DNA fragment encoding PEX3 followed by a 5-aa linker (GGGGS) and a fragment encoding mEGFP with an N-terminal 10-aa linker (GGGGSGGGGS) were cloned together into pEF-IRESpuro3 vector. The *PEX3* sequence was obtained from pcDNAZeo/*RnPEX3*, while the *mEGFP* sequence was originally prepared by introducing the monomerizing A206K mutation into pcDNAZeo/*C-EGFP* (Yagita et al., 2013) using inverse PCR.

Cell culture and cell lines

HeLa, HEK293, and their derivative cell lines were grown in DMEM (Invitrogen) supplemented with 10% FBS at 37˚C under 5% CO_2. CHO-K1 and its derivative cell lines were cultured in Ham's F-12 medium (Invitrogen) supplemented with 10% FBS under 5% CO_2. Unless otherwise indicated, cells were maintained in the absence of any antibiotics. To generate HeLa-derived and HEK293-derived cell lines, plasmid transfection was conducted using Lipofectamine 2000 (Invitrogen) according to the manufacturer's instructions. To generate CHO-K1-derived KO cell lines, plasmid transfection was carried out using Lipofectamine (Invitrogen) according to the manufacturer's instructions.

PEX16-KO clonal cell lines were generated via CRISPR/Cas9-mediated gene editing, essentially as described (Yagita et al., 2017). The gRNAs targeting exon 1 or exon 4 of the human *PEX16* gene and those targeting exon 4 of the Chinese hamster *Pex16* gene were designed using CRISPOR (http://crispor.org) (Concordet and Haeussler, 2018) (Haeussler et al., 2016) and cloned into pX330 vector (Addgene plasmid # 42230; a gift from Feng Zhang). The target sequences were as follows (see also Figs. S1-S3): hPEX16-Ex1-gRNA1, 5'-GGTGACGAGTCACGTACTCC-3'; hPEX16-Ex2-gRNA2, 5'-GGAGTACGTGACTCGTCACC-3'; hPEX16-Ex4-gRNA1, 5'-GAGCGTGCTGGAGTGCGTGG-3'; hPEX16-Ex4-gRNA2, 5'-GCTGACATGGCTGAGCGTGC-3'; hPEX16-Ex4-gRNA4, 5'-CGAGGGCGATGACAAGCCAG-3'; cPex16-Ex4-gRNA1, 5'-GCTGACATGGCTGAGCGTGC-3'; and cPex16-Ex4-gRNA2, 5'-CCATGTCAGCAACTTCTGCT-3'. The resulting pX330-based plasmids were separately transfected into HeLa, HEK293, and CHO-K1 cells, followed by single-cell cloning using limiting dilution at 0.5 cell/well into 96-well plates. After expansion, clones were screened for successful KO by genotyping and/or immunoblotting. For genotyping, genomic DNA was extracted from each clone, and a region encompassing the gRNA target sites was PCR-amplified using the following primer sets: 5'-GTGTGAGTGAGCATCTGCCT-3' and 5'-GTGGGAAGCGGTTCAAGAGA-3' for human PEX16-KO clones generated by disrupting exon 1; 5'-GTCCATCTGAGCCTCAAACC-3' and 5'-AGCCGCATCATTGTCTTCTC-3' for

human PEX16-KO clones generated by disrupting exon 4; and 5'-CTCTGCTTCTCAGTGTACTC-3' and 5'-TGCTCCAAACCCACAGATCA-3' for CHO-K1-derived Pex16-KO clones. The purified PCR products were then directly Sanger-sequenced. In the case of heterozygous mutations, the sequencing trace data were deconvoluted using TIDE webtool (http://shinyapps.datacurators.nl/tide/) (Brinkman et al., 2014). To further characterize the mutations in the PEX16-KO cell lines used in this study, the PCR product was cloned into T-Vector pMD19 (Takara Bio Inc.) and sequenced.

To generate the DKO HeLa cell lines PEX16/PEX3-DKO and PEX16/PEX19-DKO, CRISPR gRNAs targeting exon 2 of the human *PEX3* gene (5'-ATGATATTGTCGTCGTGCTT-3') and exon 1 of the human *PEX19* gene (5'-GTGTCGGGGCCGAAGCGGAC-3') were likewise designed and cloned into pX330 vector. These plasmids were individually transfected into PEX16-KO HeLa clone ex1-g1-3 cells. After single-cell cloning and expansion, clones were screened for the absence of PEX3 or PEX19 protein using immunoblotting. Genotyping was not performed. For each DKO cell line, one clone was chosen and used in the present study.

To establish PEX16/PEX19-DKO cells stably expressing HA-PEX19 (16/19-DKO$^{HA\text{-}PEX19}$), PEX16/PEX19-DKO cells were transfected with pEF-IRESpuro3/*HA-PEX19* that had been linearized with SspI restriction enzyme. The transfected cells were then selected with 0.5 µg/ml puromycin (Sigma-Aldrich) for ~2 weeks. Similarly, PEX16/PEX3-DKO cells were transfected with SspI-linearized pEF-IRESpuro3/*PEX3-mEGFP* and selected with puromycin to generate PEX16/PEX3-DKO cells stably expressing PEX3-mEGFP (16/3-DKO$^{PEX3\text{-}mEGFP}$). Single-cell cloning was not done for either of these stable cell lines, and pooled populations of puromycin-resistant cells were analyzed.

Genetic complementation assays

Cells grown in 12-well plates were transfected and analyzed as described in figure legends. The amounts of each plasmid DNA used for transfection were as follows: pcDNAZeo/*HA-PEX16* and its derivatives, 10 ng/well; pcDNA6N/*mCherryNLS-2A-HA-PEX16*, 10 ng/well; pcDNAZeo/*RnPEX3*, 100 ng/well; pcDNAZeo/*FLAG-PEX19*, 100 ng/well; pcDNA6N/*mCherryNLS-2A-FLAG-PEX19*, 100 ng/well; and pcDNA6N/*mCherryNLS-2A-PEX3*, 200 ng/well. The total amount of transfected plasmid DNA was maintained constant at 400 ng/well by adding empty pcDNA3.1/Zeo(+) vector. Lipofectamine 2000 (Invitrogen) was used at 1 µL/well to deliver plasmid DNA into HeLa-derived and HEK293-derived cells, while Lipofectamine (Invitrogen) was used at 2.4 µL/well to deliver plasmid DNA into CHO-K1-derived cells. For the experiments shown in Fig. 4, Fig. S4, Fig. S6D, and Fig. S6E, cells grown on glass coverslips were transfected and analyzed as indicated in the figure legends. For the experiments shown in Fig. 6, Fig. 7, and Fig. S6C, cells grown in 12-well plates (not on glass coverslips) were transfected as indicated in the figure legends. On the following day, transfected cells were plated on glass coverslips and further cultured until analysis.

Immunofluorescence microscopy

All immunostaining steps were performed at RT. Briefly, cells grown on glass coverslips were fixed with 4% PFA in PBS for 15 min, permeabilized with 1% Triton X-100 in PBS for 5 min, and blocked with PBS-BSA (1% BSA in PBS) for 30 min. Coverslips were then incubated with primary antibodies in PBS-BSA for 90 min and washed extensively with PBS, followed by a 60-min incubation with the appropriate Alexa Fluor-conjugated secondary antibodies diluted in PBS-BSA. After extensive washes with PBS, coverslips were rinsed with ultrapure water and mounted on slides with PermaFluor aqueous mounting medium (Thermo Fisher Scientific). Where appropriate, nuclei were stained with Hoechst 33342 during one of the washing steps after the secondary antibody incubation.

Image acquisition was performed at RT using a laser-scanning confocal microscope (LSM 710 with Axio Observer.Z1; Carl Zeiss) controlled by ZEN acquisition software. Images shown in Fig. S1A were captured using a 63×/1.40 NA i Plan-Apochromat oil immersion objective, while all the other images were acquired using a 100×/1.46 NA alpha Plan-Apochromat oil immersion objective. Linear brightness and contrast adjustments were performed using Fiji (https://fiji.sc;) (Schindelin et al., 2012) for presentation purpose, and final figures were prepared using Adobe Photoshop CS6 and Illustrator CS6. All images within one dataset were taken at the same intensity and, unless otherwise indicated, were adjusted identically.

Quantification of peroxisomal morphology

To quantify the number of peroxisomes and the average size of peroxisomes in an individual cell, 4-6 z-sections at 0.5-μm interval were obtained as described above. 2D images produced by maximum intensity projection method of ZEN 2012 software (Carl Zeiss) were then converted into threshold images. The peroxisome number and the average size of peroxisomes in an individual cell were determined using the Analyze Particles package of ImageJ 1.52a software (National Institutes of Health).

Preparation of whole cell lysates and membrane fractions for immunoblot analysis

To prepare whole cell lysates, cells were washed twice with PBS and lysed in SDS-sample buffer (62.5 mM Tris-HCl, pH6.8, 2% SDS, 10% glycerol, 5% 2-mercaptoethanol, and 0.01% bromophenol blue), followed by heating at 95˚C for 10 min with occasional vortexing to shear genomic DNA. For preparation of membrane fractions, cells were detached by trypsin treatment and then resuspended in buffer H (0.25 M sucrose, 20 mM Hepes-KOH, pH 7.4, 1 mM EDTA, and a protease inhibitor cocktail (Peptide Institute, Osaka, Japan)), followed by the homogenization on ice by passing through a 27-gauge needle (with 1mL syringe). Homogenates were centrifuged at 800× *g* for 5 min to pellet nuclei and debris, and the postnuclear supernatants were separated into cytosolic and membrane fractions by ultracentrifugation at 100,000× *g* for 30 min. The membrane fractions were dissolved in SDS-sample buffer, followed by heating at 95˚C for 10 min.

Immunoblotting

Samples were separated by SDS-PAGE and electrotransferred to a polyvinylidene fluoride membrane (Bio-Rad Laboratories) using the Mini Trans-Blot Cell (Bio-Rad Laboratories). Blots were blocked in PBS-T-milk (PBS containing 0.1% Tween 20 and 5% nonfat dry milk) for 30-60 min at RT, incubated with appropriate primary antibodies for 12-18 h at 4˚C, washed three times with PBS-T (PBS containing 0.1% Tween 20) for 10 min each, and then incubated with HRP-conjugated secondary antibodies for 60-90 min at RT. For immunoblotting with anti-HA and anti-β-actin antibodies, both primary and secondary antibodies were diluted in PBS-T-milk. For immunoblotting with anti-PEX3, anti-PEX16, and anti-PEX19 antibodies, Can Get Signal Solutions 1 and 2 (TOYOBO) were used to dilute primary and secondary antibodies, respectively. After extensive washing in PBS-T, blots were developed with Amersham ECL Prime Western Blotting Detection Reagent (GE Healthcare) and visualized using a luminescent image analyzer (LAS 4000 Mini; Fujifilm).

Quantitative real-time RT-PCR

TRIzol reagent (Invitrogen) was used for the extraction of total RNA from the cells. First-strand cDNA was synthesized using a PrimeScript RT reagent kit (Takara bio). The steady-state expression level of *PEX16* mRNA was determined by quantitative real-time RT-PCR using SYBR Premix Ex Taq II (Takara Bio) and an Mx3000P QPCR system (Agilent Technologies), and then the value was normalized to that of *GAPDH* mRNA. Primer sets used were as follows: human *PEX16*, 5'-AGCCTCCTGAGTGACAGAAAG-3' and 5'-GCAGGTAGTAGAGCAGCAGGAT-3'; human *GAPDH*, 5'-ATGGAAATCCCATCACCATCTT-3' and 5'-CGCCCCACTTGATTTTGG-3'; Chinese hamster *Pex16*-a, 5'-GAAGTTGCTGACATGGCTGA-3' and 5'-CTGGATGAGAGCAATGACGA-3'; Chinese hamster *Pex16*-b, 5'-AGCAGGAGGAGCTTAGCACA-3' and 5'-GAGAGTAGCCAGGGTGTCCA-3'; and Chinese hamster *Gapdh*, 5'-TGTGGAAGGACTCATGACCA-3' and 5'-GGATGCAGGGATGATGTTCT-3'.

Statistical analysis

Statistical analysis was performed as indicated in the figure legends using GraphPad Prism (version 9; GraphPad Software). No statistical method was used to predetermine sample size.

Acknowledgments

We thank S. Yamashita for affinity-purifying anti-PEX3 antiserum. We also thank the other members of our laboratories for helpful discussion. This work was supported in part by grants from the Ministry of Education, Culture, Sports, Science, and Technology of Japan; Grants-in-Aid for Scientific Research (JP19K07386 to Y.A.; JP26116007, JP15K14511, JP15K21743, and JP17H03675 to Y.F.); grants from the Takeda Science Foundation (to Y.F.), the Naito Foundation (to Y.F.), the

Japan Foundation for Applied Enzymology, and the Novartis Foundation (Japan) for the Promotion of Science (to Y.F.).

Competing financial interests

The authors declare that they have no competing financial interests.

Author contributions: Y. Yagita and Y. Fujiki conceptualized the project. Y. Yagita, and Y. Abe performed experiments and validation. Y. Yagita, and Y. Abe, and Y. Fujiki analyzed data. Y. Yagita and Y. Fujiki wrote the original draft of the manuscript. Y. Yagita, and Y. Abe, and Y. Fujiki reviewed and edited the manuscript.

References

Adey, A., Burton, J. N., Kitzman, J. O., Hiatt, J. B., Lewis, A. P., Martin, B. K., Qiu, R., Lee, C. and Shendure, J. (2013). The haplotype-resolved genome and epigenome of the aneuploid HeLa cancer cell line. *Nature* **500**, 207-211.

Agrawal, G. and Subramani, S. (2016). *De novo* peroxisome biogenesis: Evolving concepts and conundrums. *Biochim. Biophys. Acta-Mol. Cell Res.* **1863**, 892-901.

Baldwin, H. A., Wang, C., Kanfer, G., Shah, H. V., Velayos-Baeza, A., Dulovic-Mahlow, M., Brüggemann, N., Anding, A., Baehrecke, E. H., Maric, D. et al. (2021). VPS13D promotes peroxisome biogenesis. *J. Cell Biol.* **220**, e202001188.

Brinkman, E. K., Chen, T., Amendola, M. and van Steensel, B. (2014). Easy quantitative assessment of genome editing by sequence trace decomposition. *Nucleic acids research* **42**, e168.

Burkhart, S. E., Llinas, R. J. and Bartel, B. (2019). PEX16 contributions to peroxisome import and metabolism revealed by viable *Arabidopsis pex16* mutants. *J. Integr. Plant Biol.* **61**, 853–870.

Concordet, J.-P. and Haeussler, M. (2018). CRISPOR: intuitive guide selection for CRISPR/Cas9 genome editing experiments and screens. *Nucleic Acids Res.* **46**, W242-W245.

Ebberink, M. S., Csanyi, B., Chong, W. K., Denis, S., Sharp, P., Mooijer, P. A. W., Dekker, C. J. M., Spooner, C., Ngu, L. H., De Sousa, C. et al. (2010). Identification of an unusual variant peroxisome biogenesis disorder caused by mutations in the *PEX16* gene. *J. Med. Genet.* **47**, 608-615.

Eitzen, G. A., Szilard, R. K. and Rachubinski, R. A. (1997). Enlarged peroxisomes are present in oleic acid-grown *Yarrowia lipolytica* overexpressing the *PEX16* gene encoding an intraperoxisomal peripheral membrane peroxin. *J. Cell Biol.* **137**, 1265-1278.

Fang, Y., Morrell, J. C., Jones, J. M. and Gould, S. J. (2004). PEX3 functions as a PEX19 docking factor in the import of class I peroxisomal membrane proteins. *J. Cell Biol.* **164**, 863-875.

Farré, J.-C., Mahalingam, S. S., Proietto, M. and Subramani, S. (2019). Peroxisome biogenesis, membrane contact sites, and quality control. *EMBO Rep.* **20**, e46864.

Farré, J.-C., Carolino, K., Stasyk, O. V., Stasyk, O. G., Hodzic, Z., Agrawal, G., Till, A., Proietto, M., Cregg, J., Sibirny, A. A. et al. (2017). A new yeast peroxin, Pex36, a functional homolog of mammalian PEX16, functions in the ER-to-peroxisome traffic of peroxisomal membrane proteins. *J. Mol. Biol.* **429**, 3743-3762.

Fujiki, Y. (2016). Peroxisome biogenesis and human peroxisome-deficiency disorders. *Proc. Jpn. Acad., Ser. B* **92**, 463-477.

Fujiki, Y., Okumoto, K., Mukai, S., Honsho, M. and Tamura, S. (2014). Peroxisome biogenesis in mammalian cells. *Front. Physiol.* **5**, article 307.

Fujiki, Y., Abe, Y., Imoto, Y., Tanaka, A. J., K., O., Honsho, M., Tamura, S., Miyata, N., Yamashita, T., Chung, W. K. et al. (2020). Recent insights into peroxisome biogenesis and associated diseases. *J. Cell Sci.* **133**, jcs236943.

Ghaedi, K., Tamura, S., Okumoto, K., Matsuzono, Y. and Fujiki, Y. (2000). The peroxin Pex3p initiates membrane assembly in peroxisome biogenesis. *Mol. Biol. Cell* **11**, 2085-2102.

Guo, T., Kit, Y. Y., Nicaud, J. M., Le Dall, M. T., Sears, S. K., Vali, H., Chan, H., Rachubinski, R. A. and Titorenko, V. I. (2003). Peroxisome division in the yeast *Yarrowia lipolytica* is regulated by a signal from inside the peroxisome. *J. Cell Biol.* **162**, 1255-1266.

Guo, T., Gregg, C., Boukh-Viner, T., Kyryakov, P., Goldberg, A., Bourque, S., Banu, F., Haile, S., Milijevic, S., San, K. H. Y. et al. (2007). A signal from inside the peroxisome initiates its division by promoting the remodeling of the peroxisomal membrane. *J. Cell Biol.* **177**, 289-303.

Haeussler, M., Schönig, K., Eckert, H., Eschstruth, A., Mianné, J., Renaud, J.-B., Schneider-Maunoury, S., Shkumatava, A., Teboul, L., Kent, J. et al. (2016). Evaluation of off-target and on-target scoring algorithms and integration into the guide RNA selection tool CRISPOR. *Genome Biol.* **17**, 148.

Honsho, M., Hiroshige, T. and Fujiki, Y. (2002). The membrane biogenesis peroxin Pex16p: topogenesis and functional roles in peroxisomal membrane assembly. *J. Biol. Chem.* **277**, 44513-44524.

Honsho, M., Tamura, S., Shimozawa, N., Suzuki, Y., Kondo, N. and Fujiki, Y. (1998). Mutation in *PEX16* is causal in the peroxisome-deficient Zellweger syndrome of complementation group D. *Am. J. Hum. Genet.* **63**, 1622-1630.

Hosoi, K., Miyata, N., Mukai, S., Furuki, S., Okumoto, K., Cheng, E. H. and Fujiki, Y. (2017). The VDAC2–BAK axis regulates peroxisomal membrane permeability. *J. Cell Biol.* **216**, 709-721.

Hua, R., Gidda, S. K., Aranovich, A., Mullen, R. T. and Kim, P. K. (2015). Multiple domains in PEX16 mediate its trafficking and recruitment of peroxisomal proteins to the ER. *Traffic* **16**, 832-852.

Jean Beltran, P. M., Cook, K. C., Hashimoto, Y., Galitzine, C., Murray, L. A., Vitek, O. and Cristea, I. M. (2018). Infection-Induced Peroxisome Biogenesis Is a Metabolic Strategy for Herpesvirus Replication. *Cell Host Microbe* **24**, 526–541.e527.

Jones, J. M., Morrell, J. C. and Gould, S. J. (2004). PEX19 is a predominantly cytosolic chaperone and import receptor for class 1 peroxisomal membrane proteins. *J. Cell Biol.* **164**, 57-67.

Kim, P. K. and Mullen, R. T. (2013). PEX16: a multifaceted regulator of peroxisome biogenesis. *Front. Physiol.* **4**, 241.

Kim, P. K., Mullen, R. T., Schumann, U. and Lippincott-Schwartz, J. (2006). The origin and maintenance of mammalian peroxisomes involves a de novo PEX16-dependent pathway from the ER. *J. Cell Biol.* **173**, 521-532.

Kinoshita, N., Ghaedi, K., Shimozawa, N., Wanders, R. J. A., Matsuzono, Y., Imanaka, T., Okumoto, K., Suzuki, Y., Kondo, N. and Fujiki, Y. (1998). Newly identified Chinese hamster ovary cell mutants are defective in biogenesis of peroxisomal membrane vesicles (peroxisomal ghosts), representing a novel complementation group in mammals. *J. Biol. Chem.* **273**, 24122-24130.

Kumar, K. R., Wali, G., Davis, R. L., Mallawaarachchi, A. C., Palmer, E. E., Gayevskiy, V., Minoche, A. E., Veivers, D., Dinger, M. E., Mackay-Sim, A. et al. (2018). Expanding the spectrum of *PEX16* mutations and novel insights into disease mechanisms. *Mol. Genet. Metab. Rep.* **16**, 46–51.

Landry, J. J., Pyl, P. T., Rausch, T., Zichner, T., Tekkedil, M. M., Stütz, A. M., Jauch, A., Aiyar, R. S., Pau, G., Delhomme, N. et al. (2013). The genomic and transcriptomic landscape of a HeLa cell line. *G3 (Bethesda)* **3**, 1213–1224.

Lin, Y. C., Boone, M., Meuris, L., Lemmens, I., Van Roy, N., Soete, A., Reumers, J., Moisse, M., Plaisance, S., Drmanac, R. et al. (2014). Genome dynamics of the human embryonic kidney 293 lineage in response to cell biology manipulations. *Nat. Commun.* **5**, Article number: 4767.

Liu, Y., Yagita, Y. and Fujiki, Y. (2016). Assembly of peroxisomal membrane proteins via the direct Pex19p-Pex3p pathway. *Traffic* **17**, 433-455.

Liu, Z., Chen, O., Wall, J. B. J., Zheng, M., Zhou, Y., Wang, L., Vaseghi, H. R., Qian, L. and Liu, J. (2017). Systematic comparison of 2A peptides for cloning multi-genes in a polycistronic vector. *Sci. Rep.* **7**, 2193.

Matsuzaki, T. and Fujiki, Y. (2008). The peroxisomal membrane protein import receptor Pex3p is directly transported to peroxisomes by a novel Pex19p- and Pex16p-dependent pathway. *J. Cell Biol.* **183**, 1275-1286.

Matsuzono, Y. and Fujiki, Y. (2006). *In vitro* transport of membrane proteins to peroxisomes by shuttling receptor Pex19p. *J. Biol. Chem.* **281**, 36-42.

Matsuzono, Y., Matsuzaki, T. and Fujiki, Y. (2006). Functional domain mapping of peroxin Pex19p: interaction with Pex3p is essential for function and translocation. *J. Cell Sci.* **119**, 3539-3550.

Matsuzono, Y., Kinoshita, N., Tamura, S., Shimozawa, N., Hamasaki, M., Ghaedi, K., Wanders, R. J. A., Suzuki, Y., Kondo, N. and Fujiki, Y. (1999). Human *PEX19*: cDNA cloning by functional complementation, mutation analysis in a patient with Zellweger syndrome, and potential role in peroxisomal membrane assembly. *Proc. Natl. Acad. Sci. USA* **96**, 2116-2121.

Mukai, S., Ghaedi, K. and Fujiki, Y. (2002). Intracellular localization, function, and dysfunction of the peroxisome-targeting signal type 2 receptor, Pex7p, in mammalian cells. *J. Biol. Chem.* **277**, 9548-9561.

Nakayama, M., Sato, H., Okuda, T., Fujisawa, N., Kono, N., Arai, H., Suzuki, E., Umeda, M., Ishikawa, H. O. and Matsuno, K. (2011). *Drosophila* carrying *Pex3* or *Pex16* mutations are models of Zellweger syndrome that reflect its symptoms associated with the absence of peroxisomes. *PLoS One* **6**, e22984.

Okumoto, K., Ono, T., Toyama, R., Shimomura, A., Nagata, A. and Fujiki, Y. (2018). New splicing variants of mitochondrial Rho GTPase-1 (Miro1) transport peroxisomes. *J. Cell. Biol.* **217**, 619-633.

Opaliński, Ł., Bartoszewska, M., Fekken, S., Liu, H., de Boer, R., van der Klei, I., Veenhuis, M. and Kiel, J. A. K. W. (2012). *De novo* peroxisome biogenesis in *Penicillium chrysogenum* is not dependent on the Pex11 family members or Pex16. *PLoS ONE* **7**, e35490.

Otera, H., Okumoto, K., Tateishi, K., Ikoma, Y., Matsuda, E., Nishimura, M., Tsukamoto, T., Osumi, T., Ohashi, K., Higuchi, O. et al. (1998). Peroxisome targeting signal type 1 (PTS1) receptor is involved in import of both PTS1 and PTS2: Studies with *PEX5*-defective CHO cell mutants. *Mol. Cell. Biol.* **18**, 388-399.

Pan, D., Klare, K., Petrovic, A., Take, A., Walstein, K., Singh, P., Rondelet, A., Bird, A. W. and Musacchio, A. (2017). CDK-regulated dimerization of M18BP1 on a Mis18 hexamer is necessary for CENP-A loading. *eLife* **6**, e02137.

Schindelin, J., Arganda-Carreras, I., Frise, E., Kaynig, V., Longair, M., Pietzsch, T., Preibisch, S., Rueden, C., Saalfeld, S., Schmid, B. et al. (2012). Fiji: an open-source platform for biological-image analysis. *Nat. Methods* **9**, 676–682.

Schlüter, A., Fourcade, S., Ripp, R., Mandel, J. L., Poch, O. and Pujol, A. (2006). The evolutionary origin of peroxisomes: an ER-peroxisome connection. *Mol. Biol. Evol.* **23**, 838-845.

Schrul, B. and Kopito, R. R. (2016). Peroxin-dependent targeting of a lipid-droplet-destined membrane protein to ER subdomains. *Nat. Cell Biol.* **18**, 740-751.

Shaheen, R., Al-Dirbashi, O. Y., Al-Hassnan, Z. N., Al-Owain, M., Makhsheed, N., Basheeri, F., Seidahmed, M. Z., Salih, M. A. M., Faqih, E., Zaidan, H. et al. (2011). Clinical, biochemical and molecular characterization of peroxisomal diseases in Arabs. *Clin. Genet.* **79**, 60–70.

Shimozawa, N., Nagase, T., Takemoto, Y., Suzuki, Y., Fujiki, Y., Wanders, R. J. A. and Kondo, N. (2002). A novel aberrant splicing mutation of the PEX16 gene in two patients with Zellweger syndrome. *Biochem. Biophys. Res. Commun.* **292**, 109-112.

Smith, J. J. and Aitchison, J. D. (2013). Peroxisomes take shape. *Nat. Rev. Mol. Cell Biol.* **14**, 803-817.

South, S. T. and Gould, S. J. (1999). Peroxisome synthesis in the absence of preexisting peroxisomes. *J. Cell Biol.* **144**, 255-266.

Sugiura, A., Mattie, S., Prudent, J. and McBride, H. M. (2017). Newly born peroxisomes are a hybrid of mitochondrial and ER-derived pre-peroxisomes. *Nature* **542**, 251-254.

Tanaka, H., Okazaki, T., Aoyama, S., Yokota, M., Koike, M., Okada, Y., Fujiki, Y. and Gotoh, Y. (2019). Peroxisomes control mitochondrial dynamics and the mitochondrion-dependent apoptosis pathway. *J. Cell Sci.* **132**, jcs224766.

Tsukamoto, T., Yokota, S. and Fujiki, Y. (1990). Isolation and characterization of Chinese hamster ovary cell mutants defective in assembly of peroxisomes. *J. Cell Biol.* **110**, 651-660.

Vishwanathan, N., Bandyopadhyay, A., Fu, H. Y., Johnson, K. C., Springer, N. M. and Hu, W. S. (2017). A comparative genomic hybridization approach to study gene copy number variations among Chinese hamster cell lines. *Biotechnol. Bioeng.* **114**, 1903-1908.

Wanders, R. J. A. (2014). Metabolic functions of peroxisomes in health and disease. *Biochimie* **98**, 36-44.

Wanders, R. J. A. and Waterham, H. R. (2006). Biochemistry of mammalian peroxisomes revisited. *Annu. Rev. Biochem.* **75**, 295-332.

Waterham, H. R., Ferdinandusse, S. and Wanders, R. J. A. (2016). Human disorders of peroxisome metabolism and biogenesis. *Biochim. Biophys. Acta* **1863**, 922-933.

Wei, X., Maharjan, Y., Dorotea, D., Dutta, R. K., Kim, D., Kim, H., Mu, Y., Park, C. and Park, R. (2021). Knockdown of PEX16 induces autophagic degradation of oeroxisomes. *Int. J. Mol. Sci.* **22**, 7989.

Wurm, F. M. and Wurm, M. J. (2017). Cloning of CHO cells, productivity and genetic Stability—A discussion. *Processes* **5**, 20.

Yagita, Y., Hiromasa, T. and Fujiki, Y. (2013). Tail-anchored PEX26 targets peroxisomes via a PEX19-dependent and TRC40-independent class I pathway. *J. Cell Biol.* **200**, 651-666.

Yagita, Y., Shinohara, K., Abe, Y., Nakagawa, K., Al-Owain, M., Alkuraya, F. S. and Fujiki, Y. (2017). Deficiency of a retinal dystrophy protein, acyl-CoA binding domain-containing 5 (ACBD5), impairs peroxisomal β-oxidation of very-long-chain fatty acids. *J. Biol. Chem.* **292**, 691-705.

Yamashita, S., Abe, K., Tatemichi, Y. and Fujiki, Y. (2014). The membrane peroxin PEX3 induces peroxisome-ubiquitination-linked pexophagy. *Autophagy* **10**, 1549-1564.

Zaabi, N. A., Kendi, A., Al-Jasmi, F., Takashima, S., Shimozawa, N. and Al-Dirbashi, O. Y. (2019). Atypical *PEX16* peroxisome biogenesis disorder with mild biochemical disruptions and long survival. *Brain Dev.* **41**, 57-65.

Figures

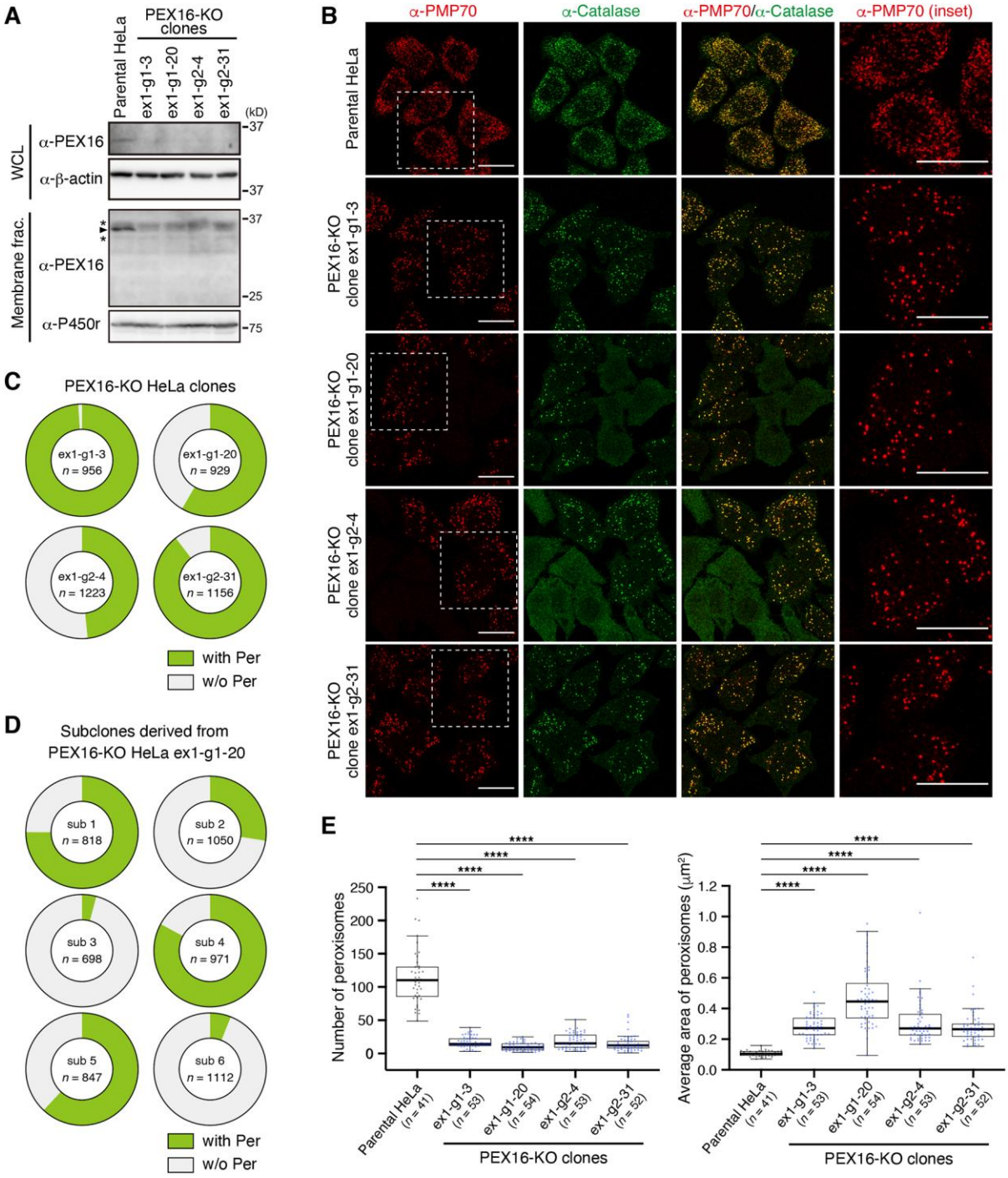

Fig. 1. Characterization of PEX16-KO HeLa cell lines. (A) Whole cell lysates (WCL, top) and membrane fractions (bottom) of parental HeLa cells and PEX16-KO HeLa clones were analyzed by immunoblotting for PEX16. β-actin and cytochrome P450 reductase (P450r), an ER membrane protein, were used as a loading control. (B) The indicated HeLa cell lines were immunostained with antibodies against PMP70 and catalase. Insets show higher-magnification images of the boxed areas.

Scale bars, 20 µm. (C) Pie charts show the proportion of cells with (with Per; green) or without (w/o Per; grey) peroxisomes in the indicated PEX16-KO clones. Cells showing catalase-positive punctate structures were counted as cells with peroxisomes. Data were collected from three independent immunostaining experiments. (D) Subclones were established from clone ex1-g1-20 and likewise analyzed for the presence of peroxisomes. Data were collected from two independent experiments and are presented as in C. (E) The number of peroxisomes per cell (left) and the average size of peroxisomes in an individual cell (right) were quantified. For simplicity, cells with PMP70-positive punctate structures were scored. Boxes represent the interquartile range (IQR), with thick lines showing the median. Whiskers extend to the minimum and maximum data points within 1.5 times IQR beyond the box. Each dot represents the value for an individual cell. Kruskal-Wallis test followed by Dunn's multiple comparisons test versus parental HeLa; ****, $p<0.0001$. *n* in C-E, total numbers of cells scored.

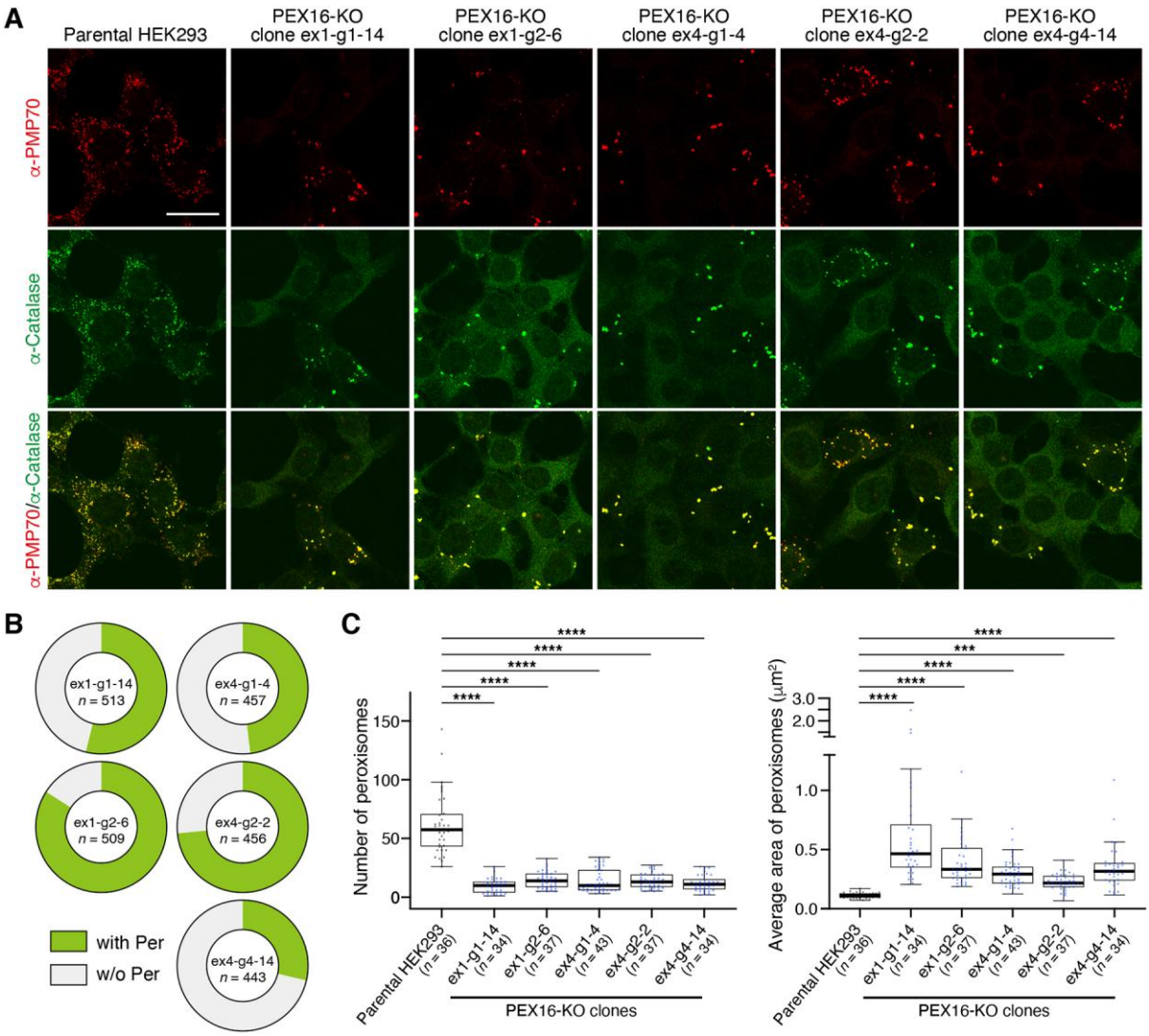

Fig. 2. Characterization of PEX16-KO HEK293 cell lines. (A) Parental HEK293 cells and the indicated PEX16-KO HEK293 clones were immunostained with antibodies against PMP70 and catalase. Scale bar, 20 µm. (B) Pie charts show the proportions of cells with (with Per; green) or without (w/o Per; grey) peroxisomes in the indicated clones. Cells showing PMP70-positive punctate structures were counted as cells with peroxisomes. (C) The number of peroxisomes per cell (left) and the average size of peroxisomes in an individual cell (right) were quantified as in Fig. 1E. Boxes, whiskers, and dots are as in Fig. 1E. Kruskal-Wallis test with Dunn's multiple comparisons test versus parental HEK293; ****, $p<0.0001$; ***, $p<0.001$. *n* in B and C, total numbers of cells scored.

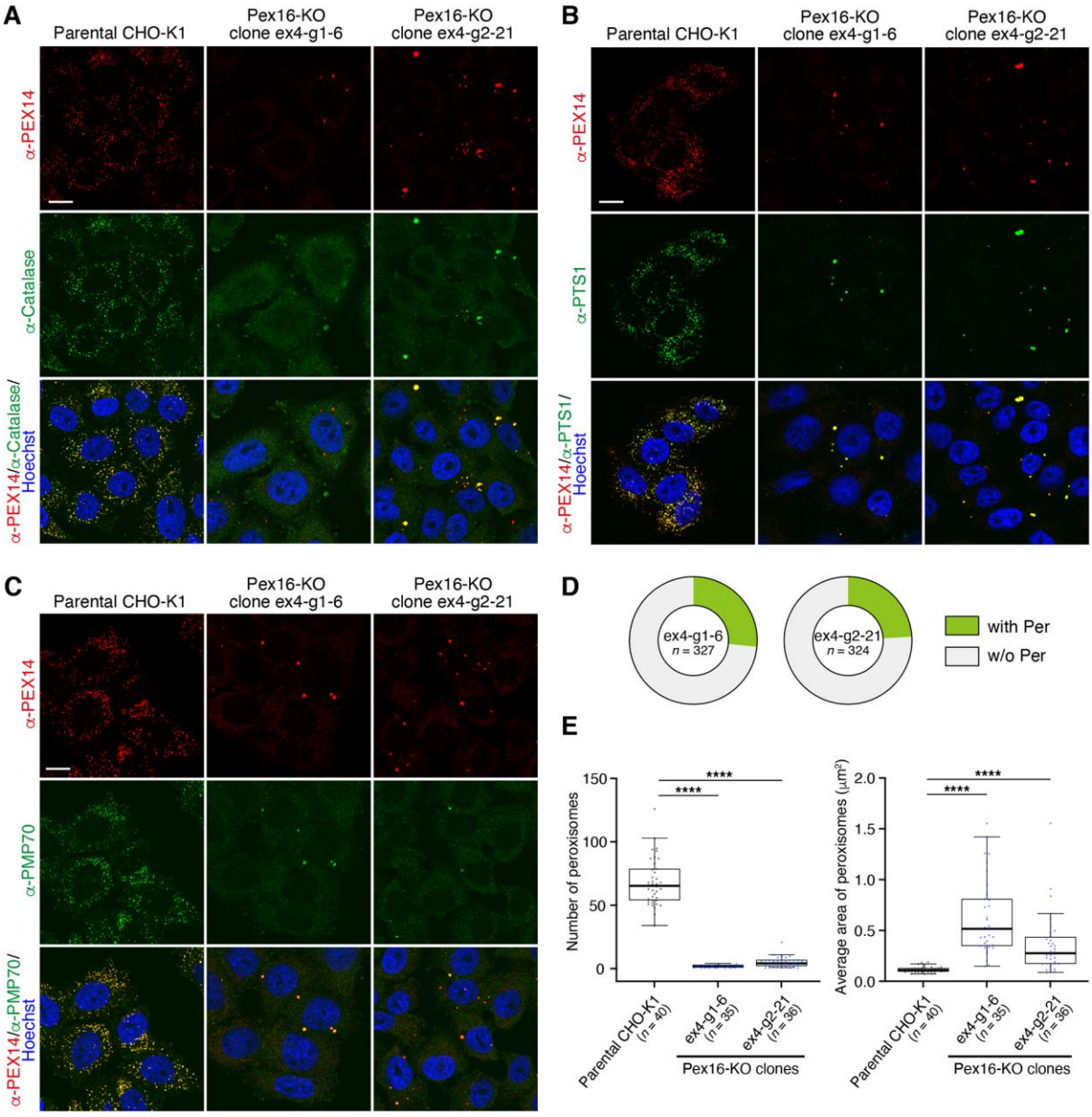

Fig. 3. Characterization of Pex16-KO CHO-K1 cell lines. (A-C) Parental CHO-K1 cells and Pex16-KO CHO-K1 clones ex4-g1-6 and ex4-g2-21 were immunostained with indicated antibodies. Scale bars, 10 μm. Note that peroxisomes in clone ex4-g1-6 were positive for a subset of matrix PTS1 proteins, whereas they barely contained catalase. (D) The proportions of cells with (with Per; green) or without (w/o Per; grey) peroxisomes in the indicated clones were quantified as in Fig. 2B. (E) The number of peroxisomes per cell (left) and the average size of peroxisomes in an individual cell (right) were quantified and are shown as in Fig. 1E. Kruskal-Wallis test with Dunn's multiple comparisons test versus parental CHO-K1; ****, $p<0.0001$. *n* in D and E, total numbers of cells scored.

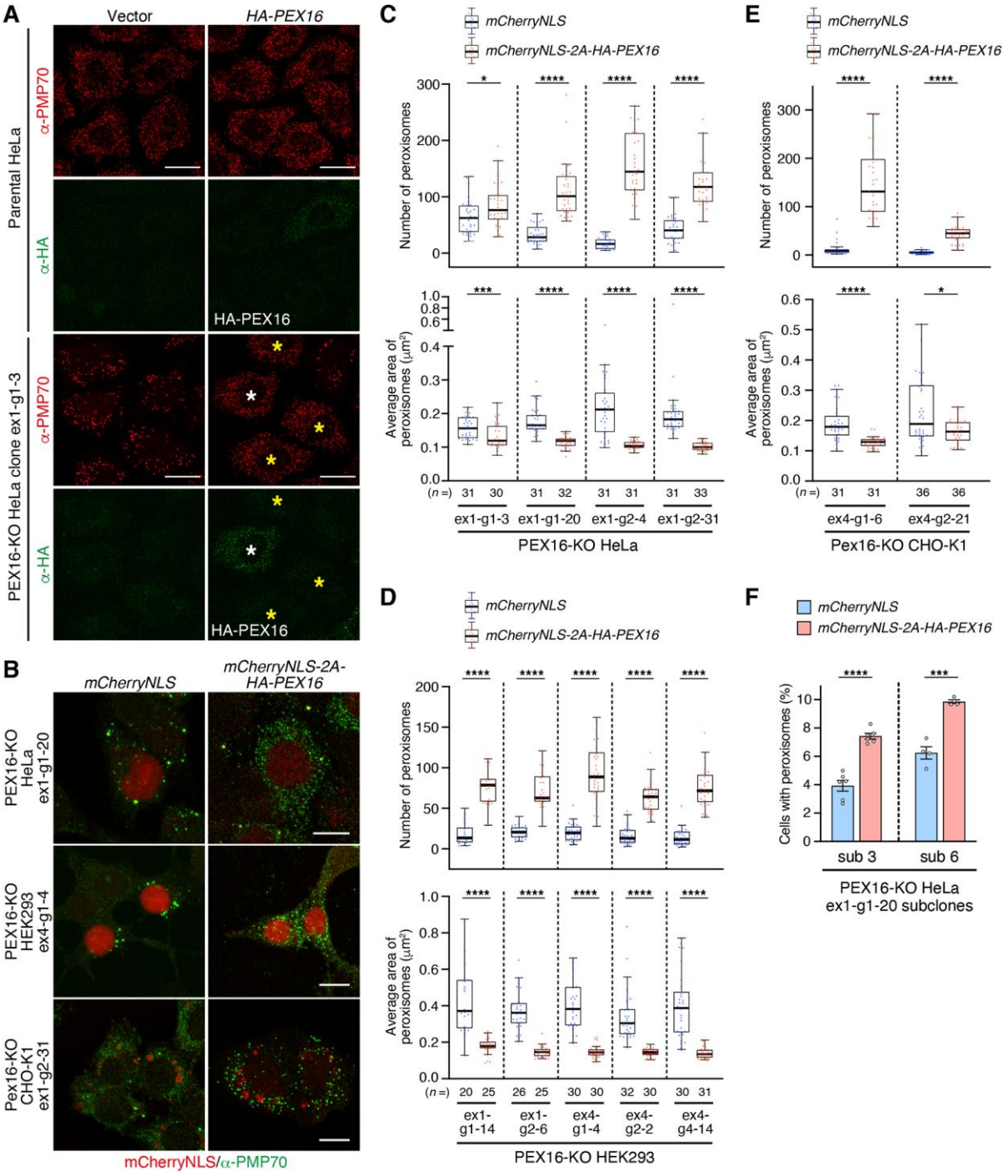

Fig. 4. Genetic complementation rescues the aberrant peroxisome morphology in PEX16-KO cell lines. (A) HeLa and PEX16-KO HeLa clone ex1-g1-3 cells were transfected with a vector or *HA-PEX16*. At 48 h after transfection, cells were fixed and immunostained with antibodies to PMP70 and HA. Note that transfection of *HA-PEX16* to PEX16-KO clone ex1-g1-3 cells restored normal peroxisome morphology not only in cells expressing detectable HA-PEX16 (white asterisk) but also in cells where HA-PEX16 was hardly visible (yellow asterisks). Scale bars, 20 µm. (B) The indicated PEX16-KO cell lines were transfected for 48 h with *mCherryNLS* or *mCherryNLS-2A-HA-PEX16* and stained for PMP70. Note that the nuclear localization of mCherryNLS was inefficient in CHO cells

for unknown reason. Scale bars, 10 µm. (C–E) PEX16-KO cell lines derived from HeLa (C), HEK293 (D), and CHO-K1 (E) were transfected and immunostained as in (B). Cells exhibiting both mCherryNLS and PMP70-positive peroxisomes were analyzed for the number of peroxisomes (upper graphs) and the average size of peroxisomes in an individual cell (lower graphs). Boxes, whiskers, and dots are as in Fig. 1E. Total numbers of cells scored (*n*) are shown. Mann-Whitney U test versus control group (mCherryNLS); ****, $p<0.0001$; ***, $p<0.001$, *, $p<0.05$. (F) Subclones 3 and 6 derived from PEX16-KO HeLa ex1-g1-20 were transfected for 4 days with *mCherryNLS* or *mCherryNLS-2A-HA-PEX16*, stained for PMP70, and analyzed for the presence of PMP70-positive peroxisomal structures. Due to undetectable level of mCherryNLS expression at the time of analysis, >500 cells were randomly scored in each experiment, and the proportion of peroxisome-positive cells was calculated. Data represent the means ± SEM of six (sub 3) and four (sub 6) independent fields of view. Dots indicate values for individual fields of views. Unpaired *t* test versus control group (mCherryNLS); ****, $p<0.0001$; ***, $p<0.001$.

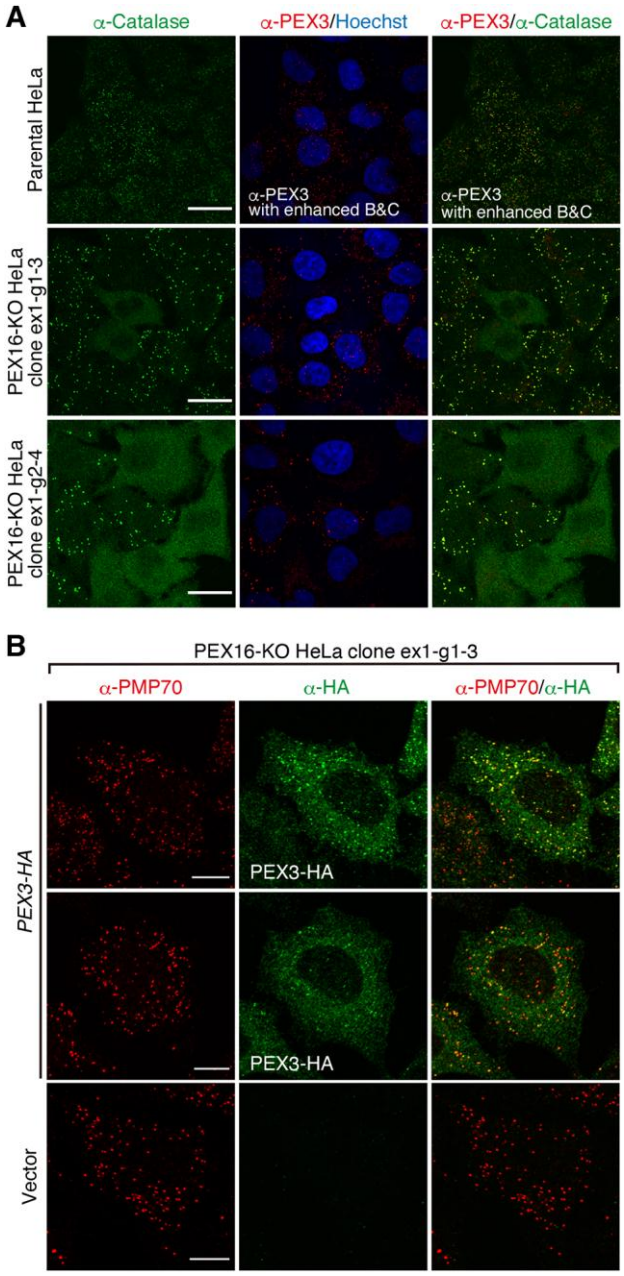

Fig. 5. PEX3 can localize to peroxisomes in PEX16-KO HeLa cells. (A) HeLa cells and PEX16-KO clones ex1-g1-3 and ex1-g2-4 were immunostained for PEX3 and catalase. Cell nuclei were stained with Hoechst 33342. Note that the anti-PEX3 antibody only very weakly detected endogenous PEX3 in wild-type HeLa cells; therefore, the PEX3 staining shown in micrographs for parental HeLa cells was digitally enhanced in brightness and contrast (enhanced B&C) to demonstrate its colocalization with catalase. Bars, 20 µm. (B) PEX16-KO clone ex1-g1-3 cells were transiently transfected with *PEX3-HA* or a vector for 48 h and then immunostained with antibodies to PMP70 and HA. Scale bars, 10 µm.

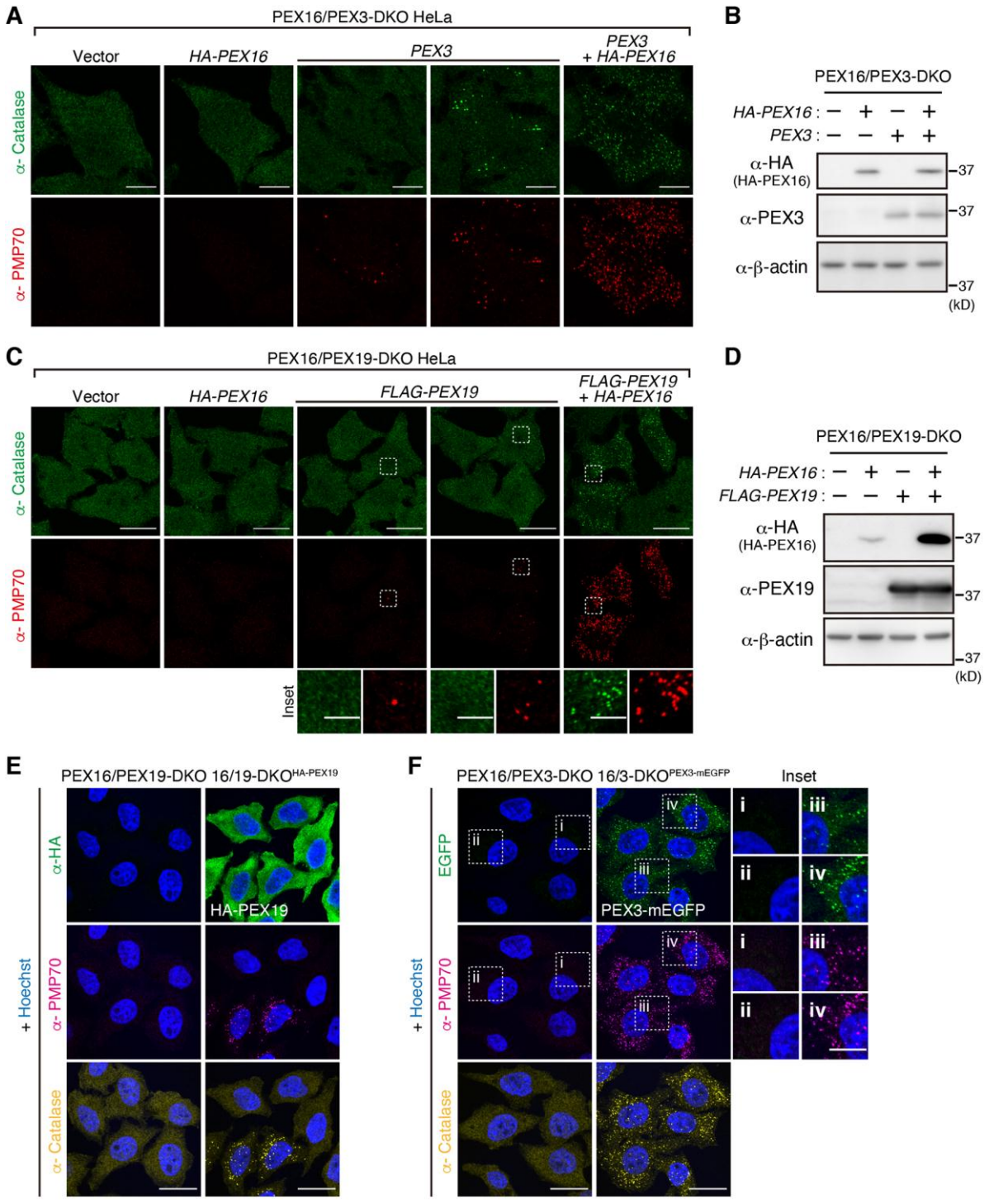

Fig. 6. PEX16 is not essential for *de novo* formation of peroxisomes. (A) PEX16/PEX3-DKO HeLa cells were transfected for 64 h with a vector, *HA-PEX16*, *PEX3*, or *PEX3* together with *HA-PEX16* and immunostained for catalase and PMP70. Scale bars, 10 µm. (B) Cell lysates from A were analyzed by immunoblotting for HA, PEX3, and β-actin. (C) PEX16/PEX19-DKO cells were transfected with a vector, *HA-PEX16*, *FLAG-PEX19*, or *FLAG-PEX19* plus *HA-PEX16*. At 64 h post-transfection, cells were fixed and immunostained as in A. Insets show higher-magnification images of the boxed areas. Scale bars, (main images) 20 µm; (insets) 5 µm. (D) Cell lysates from A were

analyzed by immunoblotting for HA, PEX19, and β-actin. Note that HA-PEX16 was stabilized by coexpressed FLAG-PEX19, as reported (Liu et al., 2016). (E) PEX16/PEX19-DKO cells and PEX16/PEX19-DKO cells stably expressing HA-PEX19 (16/19-DKO$^{HA\text{-}PEX19}$) were immunostained with antibodies against HA, PMP70, and catalase. Nuclei were stained with Hoechst 33342. Scale bars, 20 µm. (F) PEX16/PEX3-DKO cells and PEX16/PEX3-DKO cells stably expressing PEX3-mEGFP (16/3-DKO$^{PEX3\text{-}mEGFP}$) were immunostained with antibodies against PMP70 and catalase, and also stained with Hoechst 33342 for nuclei. PEX3-mEGFP was detected by EGFP fluorescence. Insets show higher-magnification images of the boxed areas. Scale bars, (main images) 20 µm; (insets) 10 µm.

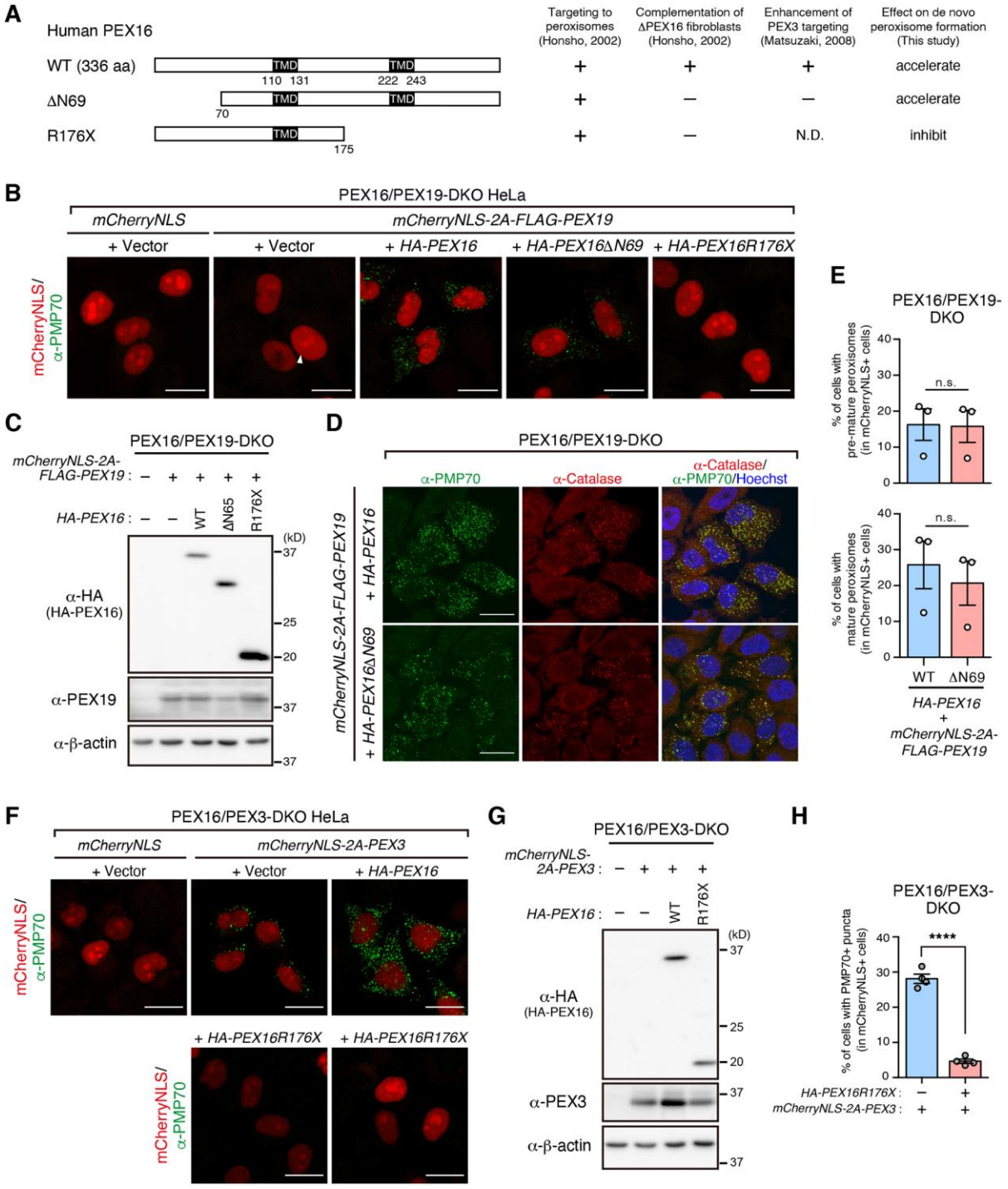

Fig. 7. C-terminal part of PEX16 is important for efficient *de novo* formation of peroxisomes. (A) Schematic view of human PEX16 and its truncation mutants. Activities of respective proteins in localizing to peroxisomes (Honsho et al., 2002), complementing *PEX16*-deficient peroxisome-less fibroblasts (Honsho et al., 2002), and enhancing the peroxisomal targeting of PEX3 *in vitro* (Matsuzaki and Fujiki, 2008) are shown on the right. Effect on *de novo* peroxisome formation, which was analyzed in B–H, is also indicated. TMD, transmembrane domain; +, active; -, inactive; N.D., not determined. (B) PEX16/PEX19-DKO HeLa cells were transfected as indicated. At 64 h after

transfection, cells were immunostained for PMP70. The arrowhead indicates a PMP70-positive structure. (C) Cells shown in B were analyzed by immunoblotting using the indicated antibodies. (D) PEX16/PEX19-DKO cells were transfected as indicated for 64 h and immunostained for PMP70 and catalase. Nuclei were stained with Hoechst 33342. (E) PEX16/PEX19-DKO cells were transfected and stained as in D, and then cells showing mCherryNLS expression were analyzed for the formation of peroxisomes. The percentages of cells with PMP70-positive but catalase-negative pre-mature peroxisomes (upper) and cells with catalase-positive mature peroxisomes (lower) are indicated. Data are the means ± SEM of three independent experiments where >150 cells were scored in each experiment. Gray dots indicate values for individual experiments. Unpaired *t* test; n.s., not significant. (F) PEX16/PEX3-DKO HeLa cells were transfected with the indicated plasmids and immunostained as in B. Two representative images are shown for cells cotransfected with *mCherryNLS-2A-PEX3* and *HA-PEX16R176X*. (G) Cells shown in F were analyzed by immunoblotting using the indicated antibodies. (H) PEX16/PEX3-DKO cells were transfected with the indicated plasmids and immunostained as in B. Cells expressing mCherryNLS were scored and assessed for the formation of PMP70-positive structures. Graph shows the percentages of cells with PMP70-positive puncta, and data represent the means ± SEM of four independent experiments where >300 cells were scored in each experiment. Grey dots indicate values for individual experiments. Unpaired *t* test; ****, $p<0.0001$. Scale bars, 20 µm.

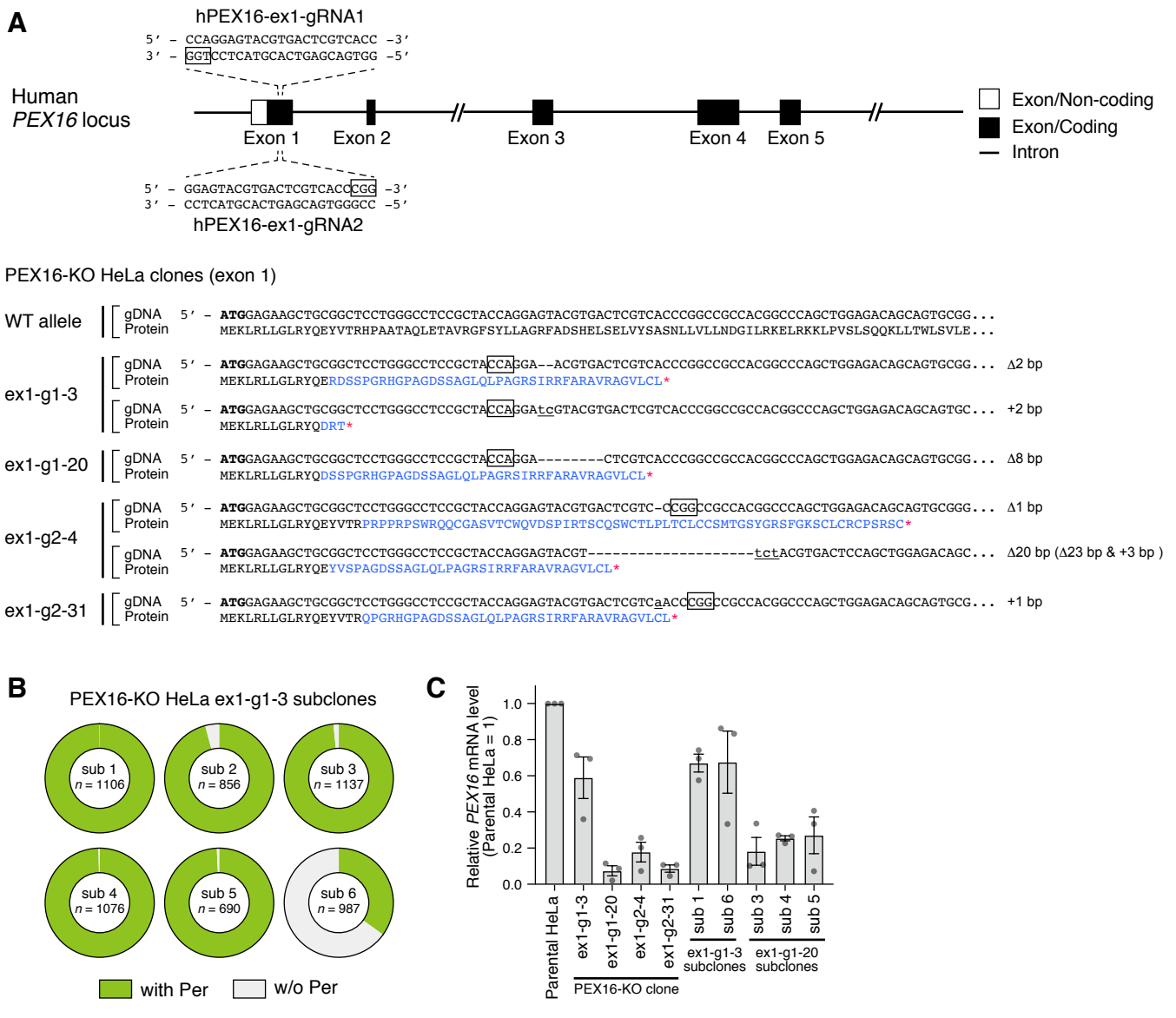

Fig. S1. Generation and characterization of PEX16-KO clonal HeLa cell lines. (A) Partial genomic structure of the human PEX16 gene (upper part) and the sequences of PEX16 alleles in PEX16-KO clones (lower part). In the diagram illustrating the genomic structure, open and filled boxes represent non-coding and coding regions in exons, respectively. Horizontal lines between boxes indicate introns. The target sequences of gRNAs in exon 1 are indicated, with the PAM sequences being boxed. In the genomic DNA sequences (gDNA), the ATG start codons are shown in bold uppercase letters, insertions are underlined, and deletions are indicated by dashes. Indel sizes (+, insertion; Δ, deletion) are also shown on the right. Deduced amino-acid sequences (protein) for each allele are also shown under the corresponding genomic sequence. The aberrant amino-acid sequences generated by frame-shift mutations are indicated in blue letters. Red asterisks mark the position where each translation terminates. Note that clones ex1-g1-3 and ex1-g1-20 were generated using hPEX16-Ex1-gRNA1, while ex1-g2-4 and ex1-g2-31 were generated with PEX16-gRNA2. (B) Pie charts showing the proportions of cells with (with Per; green) or without (w/o Per; grey) peroxisomes in six subclones established from clone ex1-g1-3. Cells showing catalase-positive punctate structures were counted as cells with peroxisomes. Data were collected from two independent. *n*, total number of cells counted. (C) Relative *PEX16* mRNA levels in PEX16-KO HeLa clones and subclones. *PEX16* mRNA levels were determined by quantitative real-time PCR, normalized to the level of *GAPDH* mRNA, and are expressed relative to the value for parental HeLa cells. Date shown are the means ± SEM of three independent experiments. Dots indicate individual data points.

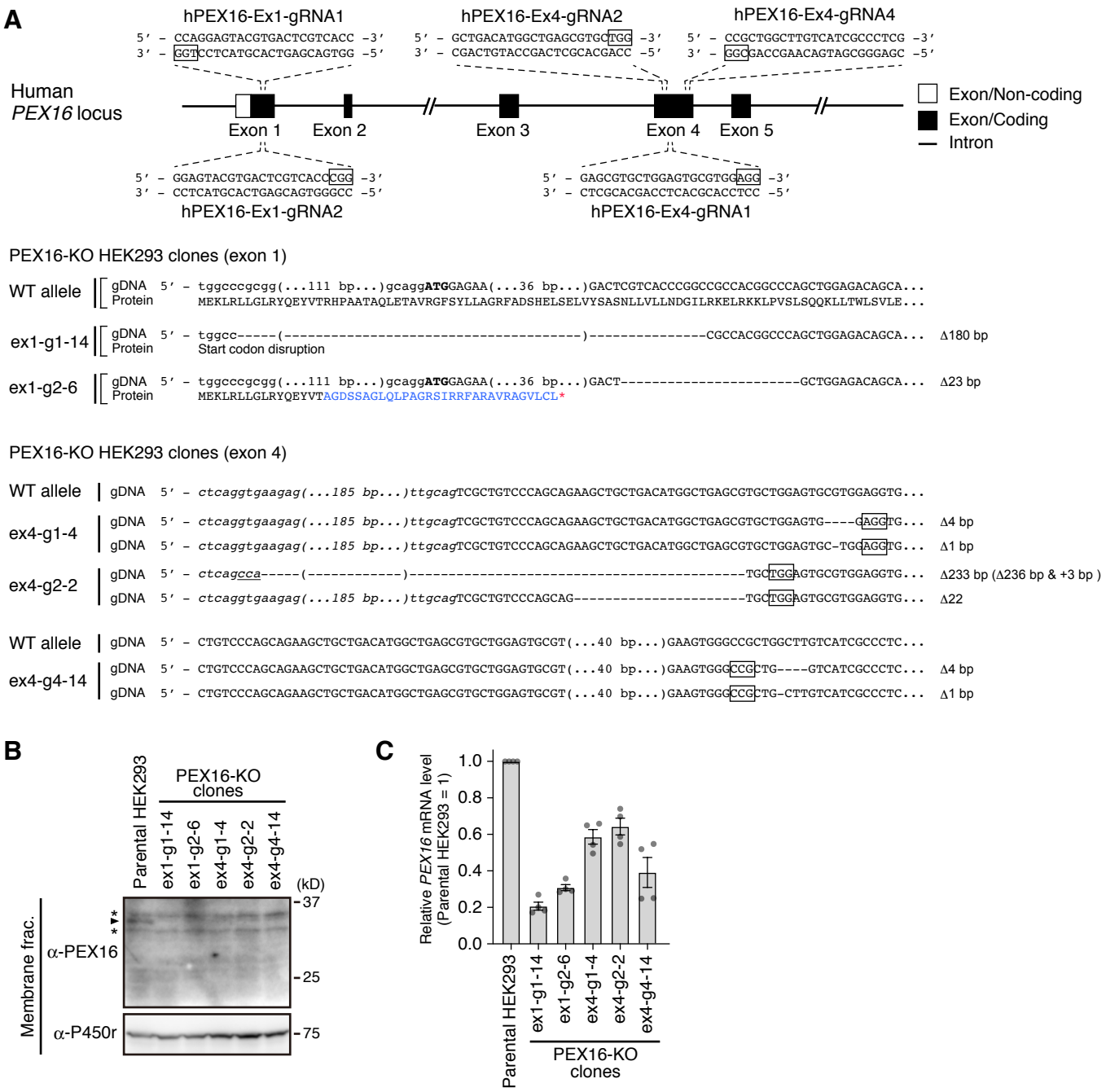

Fig. S2. Generation and characterization of PEX16-KO clonal HEK293 cell lines. (A) Partial genomic structure of the human PEX16 gene (upper part) and the sequences of PEX16 alleles in PEX16-KO clones (lower part). Diagrams and sequences are shown as in Fig. S1A. The genomic DNA (gDNA) sequences are depicted as follows: ATG start codon, bold uppercase; coding region, uppercase; non-coding region in exon 1, lowercase; and intron, italic lowercase. The sequences of the regions in parentheses are not depicted. Insertions and deletions are indicated as in Fig. S1A. Deduced amino-acid sequences (protein) were shown only for the clones generated by disrupting exon 1. Note that individual clones were made using the following gRNAs: ex1-g1-14, hPEX16-Ex1-gRNA1; ex1-g2-6, hPEX16-Ex1-gRNA2; ex4-g1-4, hPEX16-Ex4-gRNA1; ex4-g2-2, hPEX16-Ex4-gRNA2; and ex4-g4-14, hPEX16-Ex4-gRNA4. (B) Immunoblot analysis of PEX16-KO HEK293 cell lines. Membrane fractions of the indicated HEK293 cell lines were analyzed by immunoblotting for PEX16 and cytochrome P450 reductase (P450r), an ER membrane protein. (C) Relative *PEX16* mRNA levels in PEX16-KO HEK293 clones. Relative *PEX16* mRNA levels were determined as in Fig. S1C and are expressed relative to the value for parental HEK293 cells. Date shown are the means ± SEM of three independent experiments, with dots indicating individual data points.

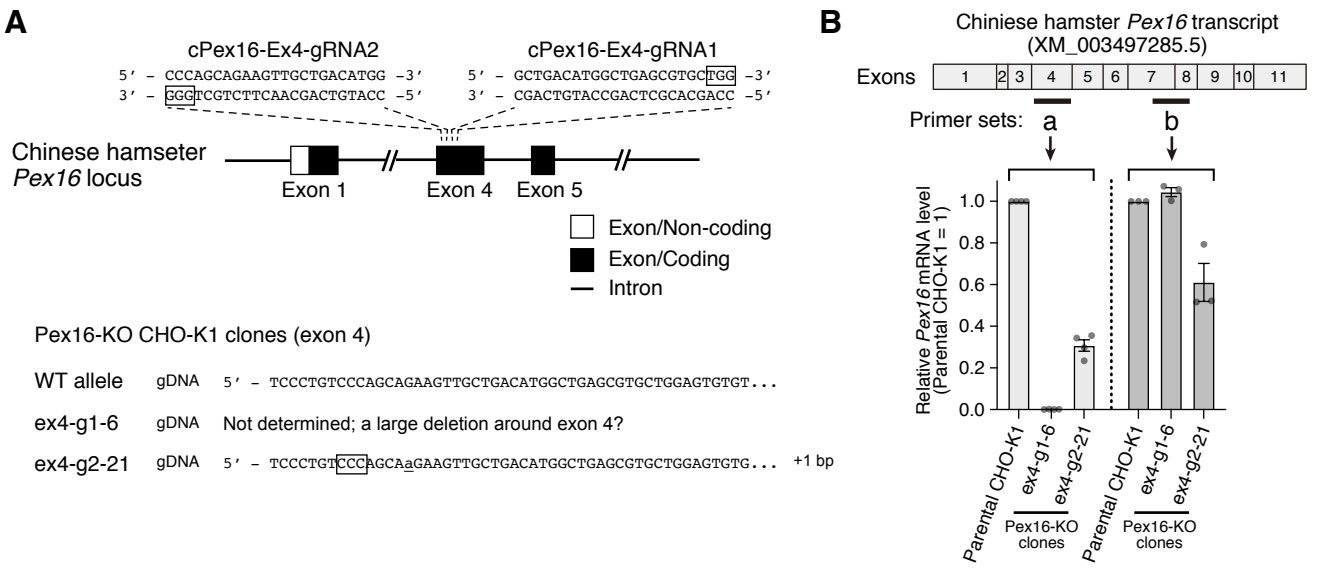

Fig. S3. Generation and characterization of Pex16-KO clonal CHO-K1 cell lines. (A) Partial genomic structure of the Chinese hamster PEX16 gene (upper part) and the sequences of PEX16 alleles in Pex16-KO clones (upper part). Diagrams and genomic DNA sequences are shown as in Fig. S1A. Note that clones ex4-g1-6 and ex4-g2-21were generated using cPex16-gRNA1 and cPex16-gRNA2, respectively. (B) Relative *Pex16* mRNA levels in Pex16-KO CHO-K1 clones. Graph shows the means ± SEM of three independent experiments, with dots indicating individual data points. Two sets (a and b) of *Pex16*-specific PCR primers were used. The PCR target regions are shown by thick bars in the diagram, where boxes and numbers indicate the exon structure of the *Pex16* transcript XM_003497285.5.

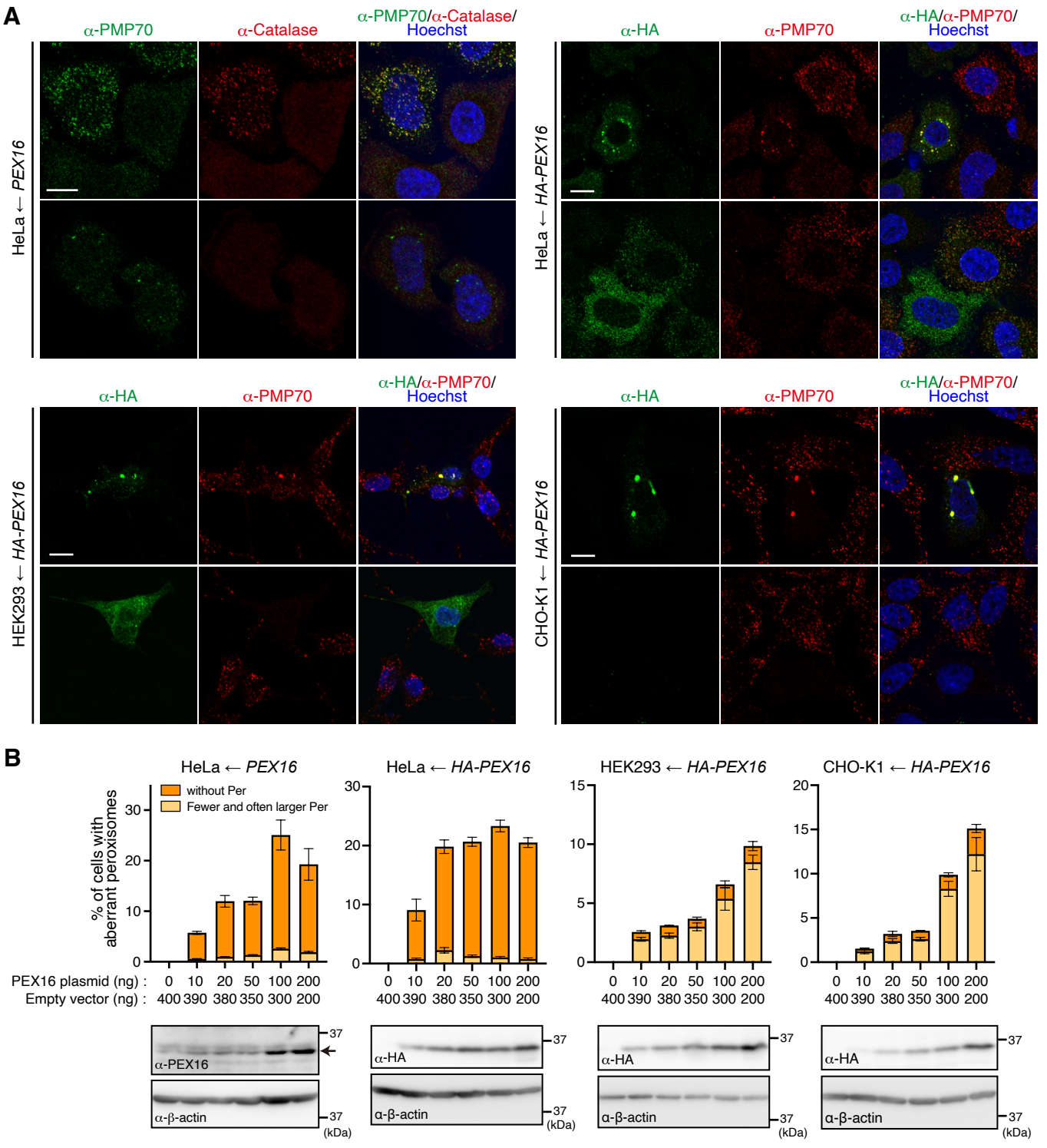

Fig. S4. Optimization of transfection conditions for transient expression of PEX16. (A) Representative images of cells transiently expressing PEX16. HeLa cells (upper panels), HEK293 cells (lower left panels), and CHO-K1 cells (lower right panels) were transfected with a plasmid encoding untagged PEX16 (*PEX16*) or HA-tagged PEX16 (*HA-PEX16*) as indicated. At 48 h post-transfection, cells were immunostained with the indicated antibodies. Nuclei were counterstained with Hoechst 33342. Note that the transient expression of PEX16 resulted in cells with fewer peroxisomes (<30 per cell in HeLa and HEK293; <20 per cell in CHO-K1) and in severe cases resulted in complete loss of peroxisomes. Note also that peroxisomes in PEX16-overexpressing cells are often larger in size, particularly in HEK293 and CHO-K1 cells. Scale bars, 10 µm. (B) Quantification of cells showing morphologically aberrant peroxisomes upon transient expression of PEX16. HeLa, HEK293, and CHO-K1 cells cultured in 12-well plates were transfected with the indicated amounts of empty vector and PEX16 or HA-PEX16 for 48 h. Cells were then immunostained for PMP70 and analyzed for peroxisomal morphology. Graphs show the fractions of cells showing fewer and often larger peroxisomes (light orange) and cells lacking peroxisomes (orange) in randomly selected cells. Data are the means ± SEM of three or four different fields of view. Total numbers of cells scored are >700 per condition (typically ~2000). Cell lysates were also analyzed by immunoblotting as indicated (bottom).

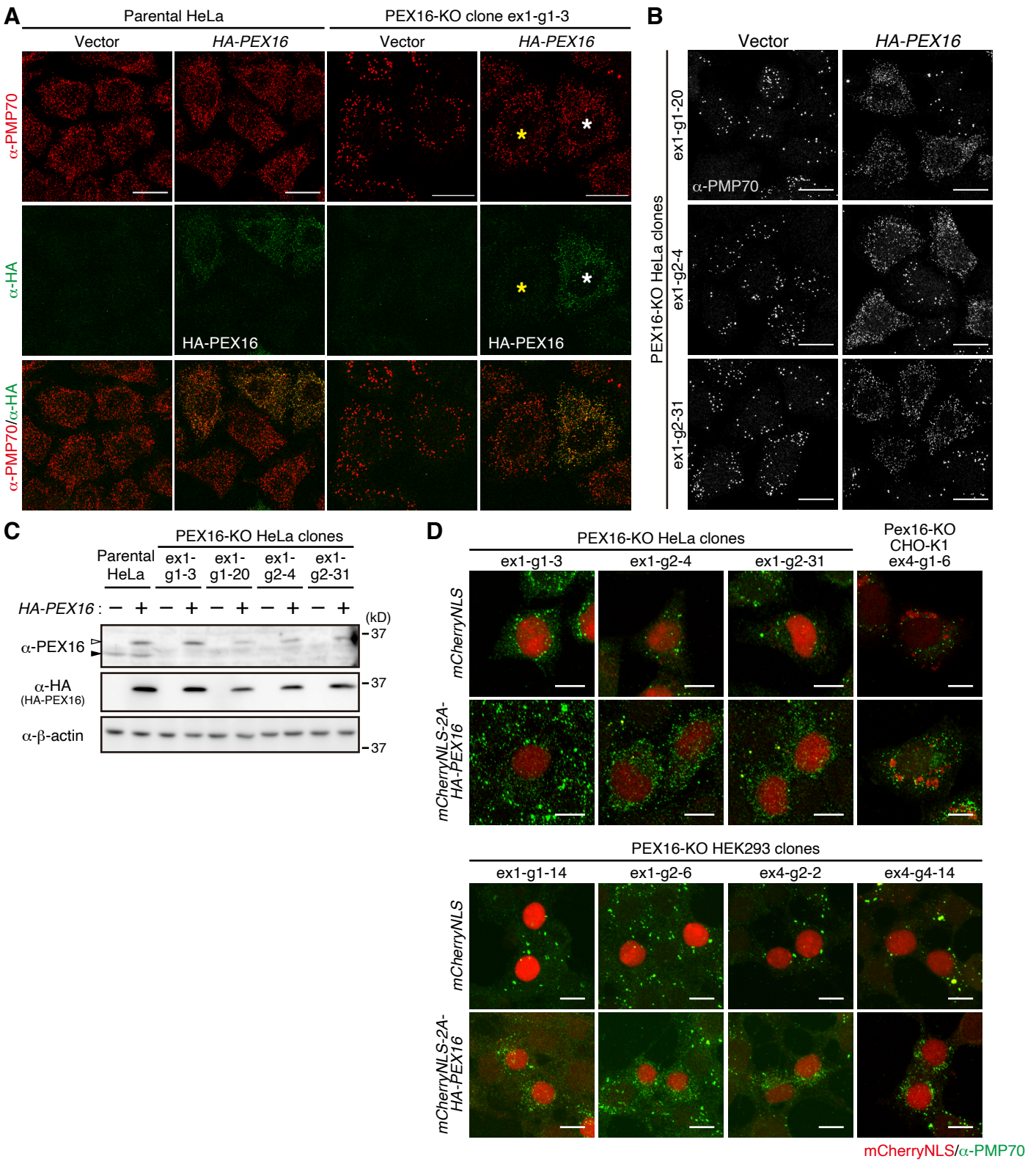

Fig. S5. Restoration of normal peroxisome morphology in PEX16-KO HeLa cells by low-level transient expression of wild-type PEX16. (A) Additional representative images of parental HeLa and PEX16-KO HeLa clone ex1-g1-3 cells transiently expressing HA-PEX16 at low levels. Cells were transiently transfected with vector or HA-PEX16 for 48 h (see also Materials and Methods for details) and then immunostained with antibodies against PMP70 and HA. The white asterisk indicates a cell showing a detectable level of HA-PEX16, while the yellow asterisk depicts a cell with a hardly detectable HA-PEX16. Note that both of these cells showed the restoration of normal peroxisome morphology. (B) Representative images of the indicated PEX16-KO clones transiently expressing HA-PEX16. Cells were transiently transfected as in A and immunostained for PMP70. (C) Immunoblotting showing expression of HA-PEX16. Cells shown in A and B were lysed and analyzed by immunoblotting for PEX16, HA, and β-actin. The open and filled arrowheads point to exogenous and endogenous PEX16 proteins, respectively. (D) Representative images of PEX16-KO cells transiently transfected with mCherryNLS-2A-HA-PEX16. The indicated PEX16-KO cell lines were transfected for 48 h with mCherryNLS or mCherryNLS-2A-HA-PEX16 and stained for PMP70. Note that the nuclear localization of mCherryNLS was inefficient in CHO cells for unknown reason. Scale bars, (A and B) 20 µm; (D) 10 µm.

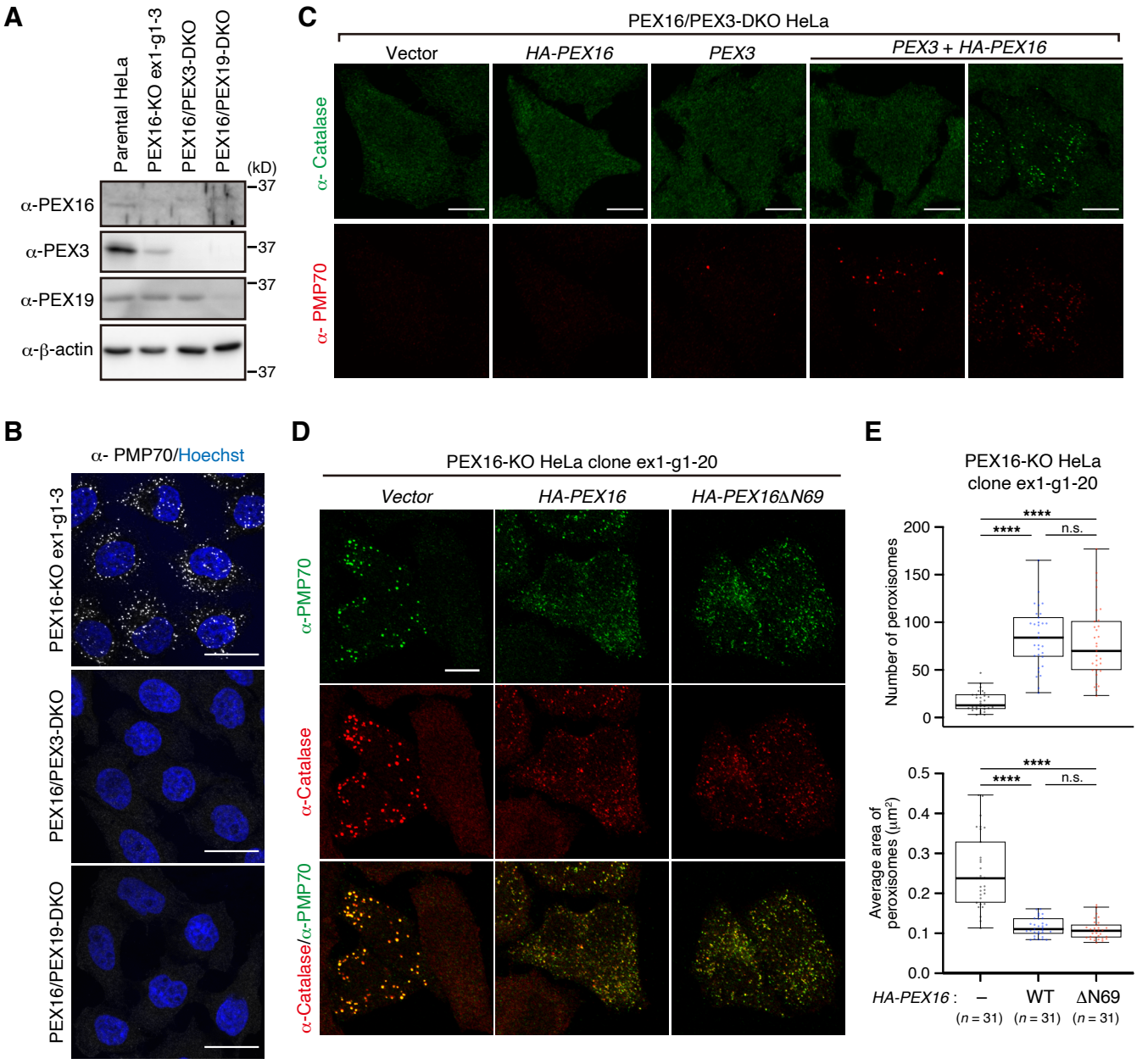

Fig. S6. PEX16 is not required for, but can accelerate, *de novo* formation of peroxisomes. (A) Characterization of PEX16/PEX3-DKO and PEX16/PEX19-DKO cells by immunoblotting. Cell lysates of the indicated cell lines were analyzed by SDS-PAGE and immunoblotting with antibodies against PEX3, PEX19, PEX16, and β-actin. (B) Representative images of PEX16/PEX3-DKO and PEX16/PEX19-DKO cells. The indicated cells were immunostained for PMP70 (white) and stained with Hoechst 33342 for nuclei (blue). (C) Representative images of PEX16/PEX3-DKO cells upon genetic complementation. PEX16/PEX3-DKO cells were transfected with a vector, HA-PEX16, PEX3, or PEX3 together with HA-PEX16. Cells were fixed at 48 h post-transfection and immunostained for catalase and PMP70. (D) Representative images of PEX16-KO HeLa cells expressing HA-PEX16ΔN69. PEX16-KO HeLa ex1-g1-20 cells were transfected for 48 h with vector, HA-PEX16, or HA-PEX16ΔN69 and then immunostained for PMP70 and catalase. (E) Quantification of peroxisomal morphology in PEX16-KO HeLa cells expressing HA-PEX16ΔN69. PEX16-KO HeLa ex1-g1-20 cells were processed as in D. The number of peroxisomes (upper) and the average size of peroxisomes in an individual cell (lower) were quantified. Cells with peroxisomes were randomly scored. Boxes denote the 25th, 50th, and 75th percentiles, while whiskers extend to the last data point within 1.5 times interquartile range beyond the box. Total numbers of cells scored (*n*) are shown. Kruskal-Wallis test with Dunn's multiple comparisons test: ****, $p<0.0001$; n.s., not significant. Scale bars, (A) 20 μm; (C and D) 10 μm.